AGU PUBLICATIONS

JGR

Journal of Geophysical Research: Earth Surface

RESEARCH ARTICLE
10.1002/2013JF003004

Key Points:
- Grain-scale diagenetic variations modulate landscape-scale form and process
- Low fracture density limits soil production via tree roots
- Assuming uniform rock properties for geomorphic modeling may be perilous

Supporting Information:
- Readme
- Figures S1 and S2

Correspondence to:
J. A. Marshall,
jillm@uoregon.edu

Citation:
Marshall, J. A., and J. J. Roering (2014), Diagenetic variation in the Oregon Coast Range: Implications for rock strength, soil production, hillslope form, and landscape evolution, *J. Geophys. Res. Earth Surf.*, *119*, 1395–1417, doi:10.1002/2013JF003004.

Received 8 OCT 2013
Accepted 9 MAY 2014
Accepted article online 13 MAY 2014
Published online 27 JUN 2014

Diagenetic variation in the Oregon Coast Range: Implications for rock strength, soil production, hillslope form, and landscape evolution

Jill A. Marshall[1] and Joshua J. Roering[1]

[1]Department of Geological Sciences, University of Oregon, Eugene, Oregon, USA

Abstract The mechanisms by which lithology modulates geomorphic processes are poorly known. In the Oregon Coast Range (OCR), rhythmically bedded sandstones of the Eocene Tyee Formation underlie steep, soil-mantled hillslopes, with relatively uniform ridge-valley spacing. These characteristic landforms are perturbed where diagenetic variations manifest as resistant cliffs. Here we use petrology, rock mechanics, and lidar to characterize grain-scale variations in rock properties and their influence on rock strength, hillslope processes, and landscape morphology in two adjacent watersheds. Petrographic analyses suggest that a suite of diagenetic products in the "resistant" bedrock account for a 2.5 times increase in tensile strength relative to "typical" Tyee bedrock. Our reference catchment exhibits negligible resistant outcrops, and consistent hillslope gradients and longitudinal valley profiles. By contrast, the adjacent catchment teems with resistant, 1 to 10 m thick, noncontiguous sandstone beds that form hanging valleys with gentle upstream hillslopes and anomalously narrow valleys. Mechanical and topographic analyses suggest that the low fracture density characteristic of these resistant beds may render them relatively impervious to comminution by tree root activity, the dominant OCR soil production mechanism. Based on both hillslope gradient- and hilltop curvature-erosion models, we estimate that hillslopes perched above resistant beds erode at approximately half the pace of hillslopes unencumbered by downstream knickpoints. The diagenetic variations likely influence relief at the watershed scale. Depositional position and diagenetic processes appear to control the occurrence of resistant beds, providing a framework to quantify how seemingly subtle variations in rock properties can impose first-order controls on landscape form and evolution.

1. Introduction

In addition to tectonics and climate, it is oft stated that lithology is a fundamental control on landscape evolution. Intuitively, we expect that harder rock will resist erosion such that all else being equal, harder rock will tend to produce steeper slopes. This simple observation is not limited to those with geologic expertise as nonscientists frequently surmise that rock hardness shapes landscapes. When Nathanial *Hawthorne* [1854], an American novelist of the seventeenth century, wrote "Mountains are Earth's undecaying monuments," he captured the concept that harder rock endures and underlies the Earth's rugged high points. In the scientific literature, *Gilbert* [1877], in his seminal work on the Henry Mountains, conceptualized process laws to describe observed patterns in landscape concavities, declivities, and divides, but he also noted how hard rocks caused deviations from these patterns. Strictly speaking, Gilbert observed that the main factors that control erosion rates are declivity (gradient), climate, and the character of the rock, with softer rocks weathering more rapidly than hard ones. Of Mount Ellsworth, Gilbert noted that the mountain "survives the general degradation of the country only in virtue of its firmer rock masses." While lithologic control on landscape evolution has been noted by many observers, functional relationships between rock properties, geomorphic processes, and landscape form have seldom been tested, and surprisingly little progress has been made since Gilbert first penned his observations on hard rock, weathering, and topographic form.

Rock strength indices, including strength tests (e.g., Schmidt hammers) and other proxies based on lithologic classification and fracture characteristics [e.g., *Selby*, 1993], have been used to explain rock controls on hillslope relief [*Schmidt and Montgomery*, 1995], landslide frequency and magnitude [*Korup and Schlunegger*, 2009; *Clarke and Burbank*, 2010], alpine cliff retreat rates [*Moore et al.*, 2009], topographic metrics [*Hurst et al.*, 2013b], and basin sediment yield [*Aalto et al.*, 2006]. With the exception of *Aalto et al.* [2006], who adapted a lithologic index for sediment yield data, a framework for making predictions and parameterizing models

based on these studies is lacking and few studies have analyzed variations within a given watershed to better constrain the role of rock properties. *Hack* [1957, 1973] recognized the role of a resistant quartzite ridge in "propping up" local Appalachian base level thus leading to changes in channel profile form. *Ahnert* [1987] inserted zones of resistant rock within a 1-D hillslope evolution model and concluded that denudation rates must exceed the resistant rock weathering rates to influence hillslope form. By contrast, measured soil production rates can vary widely with depth and rock hardness, suggesting a more complex relationship between hillslope weathering processes, bedrock strength, and form [*Heimsath et al*., 2001].

Duvall et al. [2004] collected over 1000 Schmidt hammer measurements in channels crossing both resistant and nonresistant sedimentary units and found channel concavity and steepness index values exceeding those predicted by the stream incision model for streams without lithologic variation. Using a Schmidt hammer, *Stock and Dietrich* [2006] documented along-channel strength variations related to rock properties, weathering, and debris flow frequency. *Allen et al*. [2013] used a Schmidt hammer, hand compression, and hammer blows to estimate rock strength in rivers along the Himalayan front crossing weak to resistant lithologic units and found that substrate strength influences channel form and width, with narrow channels forming upstream of resistant knickpoints. Surprisingly, none of these studies explored the actual rock properties that facilitated these geomorphic patterns, and few questioned the degree to which lithologic variation modulates landscape evolution. As a result, we have little predictive capability to foresee when rock property contrasts become geomorphically relevant.

Spatially extensive high-resolution (~1 m) digital elevation models (DEMs) are increasingly being used to evaluate hypotheses on functional relationships between form and process [e.g., *Heimsath et al*., 1997; *Dietrich et al*., 2003; *Roering et al*., 2007; *Roering*, 2008; *Perron et al*., 2009; *Gabet and Mudd*, 2010; *Hurst et al*., 2012], ecosystem services [*May et al*., 2013], and the signature of soil production mechanisms [*Roering et al*., 2010]. However, process models in use since the 1990s [e.g., *Dietrich et al*., 2003] typically ignore lithologic variations when considering attributes that control bedrock-to-soil conversion or denudation. In reality, as every geologist learns after placing nose to rock, when we step away from our maps and modeled landscapes and into the field, apparently uniform bedrock often varies in ways both obvious and subtle, ranging from visible differences in fracture density or grain size to microscopic petrologic variations. Thus, it is worth asking —when applying geomorphic process laws—is it appropriate to ignore lithologic variations?

In this study, we focus on two adjoining watersheds, within a single geologic unit, in the central portion of the well-studied Oregon Coast Range (Figure 1). We explore how previously discounted variations in rock properties control geomorphic processes and thus landscape evolution. Regionally, patches of unfractured, unvegetated rock, characterized by loggers as "bedrock meadows," ecologists as "rocky balds" [e.g., *Aldrich*, 1972; *Franklin and Dyrness*, 1988], and land managers as "nontimber producing patches" crop out amongst the soil-mantled, closed-canopy fir forests of the Oregon Coast Range. We first describe the geologic and depositional setting responsible for producing variations in rock properties. We then present observations and analyses from fieldwork, petrology, rock mechanics, and airborne lidar to characterize differences in rock properties, geomorphic processes, and topographic attributes. This paper explores how minor, grain-scale differences in rock properties that account for a relatively small percentage of hillslope length and occur discontinuously throughout a watershed can modulate bedrock-to-soil conversion processes, channel form and incision rates, subcatchment erosion rates, and catchment-scale relief.

2. Study Area: Sink to Source to Sink

2.1. The Oregon Coast Range—Geologic Setting

Our study area watersheds, Franklin and Harvey, are located in the central Oregon Coast Range and drain directly into the Umpqua River just west of Scottsburg. The Oregon Coast Range (OCR) is an unglaciated, humid soil-mantled landscape characterized by steep, highly dissected mountains [*Dietrich and Dunne*, 1978; *Reneau and Dietrich*, 1991]. The underlying deposits of the Eocene Tyee basin include trench and rift margin sediments and overlying forearc basin fill deposits that accumulated as the region transitioned from a dominantly convergent tectonic regime to a broad forearc basin. The Tyee Formation also includes overlying delta deposits commensurate with a reduction in sedimentation rates during the late Oligocene growth of the Cascade volcanic arc [*Heller et al*., 1987; *Ryu and Niem,* 1999]. The rhythmically bedded Eocene turbidity deposits of the Tyee Formation overly a thick accreted volcanic basement termed Siletzia [*Orr et al*., 1992].

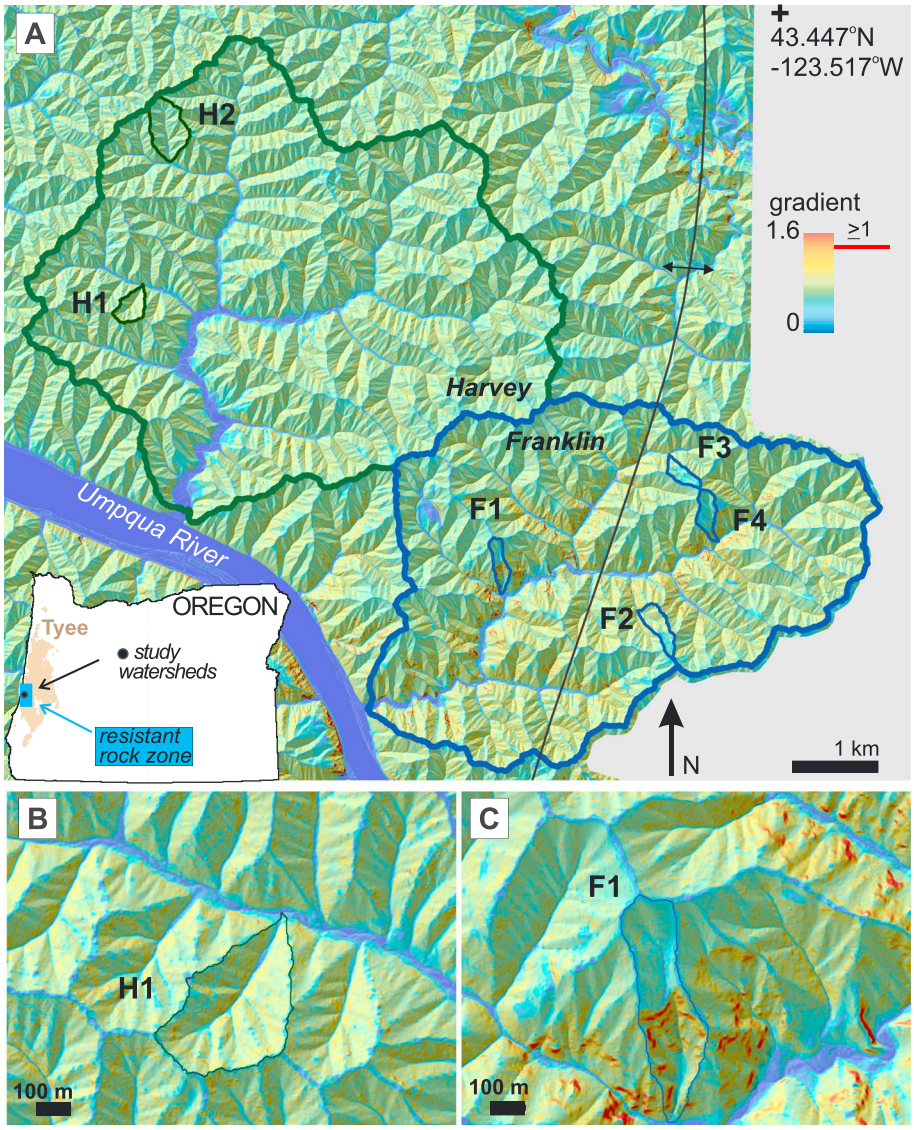

Figure 1. (a) Lidar-derived gradient map of Harvey and Franklin watersheds with individual study catchments identified for Harvey watershed in green and with H identifiers and for Franklin watershed in blue with F identifiers. Resistant rock beds are defined as having a gradient > 1 (100%) and are delineated by red tones on the map. Approximate location of anticline axis is described by thin curved line bisecting Franklin watershed from NW to SSE. Inset map delineates the extent of the Tyee Formation in tan and the general extent of resistant beds in blue, and a closed circle marks the study area location. (b) Close-up of Harvey catchments, including H1 catchment outlined in green on the gradient map. Note the topography, with catchments of uniform size and shapes with well-ordered drainage networks. (c) Close-up of Franklin catchments, including the F1 catchment outlined in blue on the gradient map. Note the disorganized topography, with low-gradient basins perched above the red bands defining resistant rock beds, varied sized and shaped catchments, and variable valley density. "Typical" Tyee bedrock underlies the soil-mantled basins perched above the resistant rock beds.

The Tyee Formation extends over 10,000 km^2 and has been studied in detail due to its distinct, well-exposed assemblage of sedimentary facies [*Snavely et al.*, 1964; *Heller and Ryberg*, 1983; *Heller and Dickinson*, 1985; *Lovell and Rogers*, 1969] and reservoir potential [*Rogers*, 1969; *Ryu and Niem*, 1999]. The turbidite beds formed from a series of delta-fed channels at the base of submarine ramps along the continental slope such that lateral (east-west) and facies variability is minimal [*Heller and Dickinson*, 1985]. The lithology is remarkably uniform [e.g., *Snavely et al.*, 1964; *Dott*, 1966; *Lovell and Rogers*, 1969] with a proximal to distal, south to north reduction in formation thickness and sand to siltstone ratio [*Lovell*, 1969]. The ~3 km thick formation [*Snavely et al.*, 1964] contains sand-rich, arkosic lithic material sourced from the Idaho batholith, mixed with immature

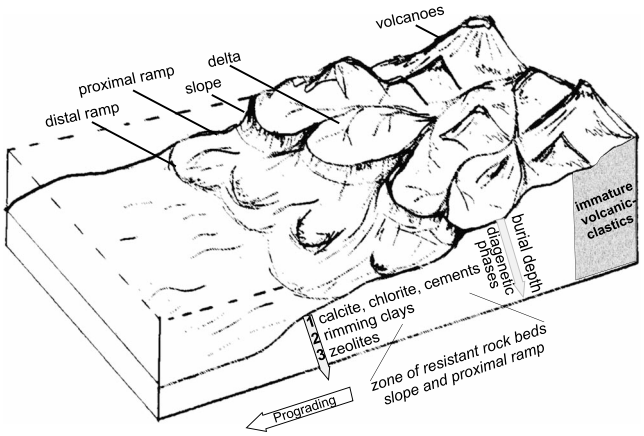

Figure 2. Conceptual model illustrating the Oregon Coast Range delta-fed submarine ramp setting during initial Eocene turbidite deposition along with the diagenetic phases found in the sand-rich slope and proximal ramp deposits underlying Franklin and Harvey watersheds. Figure based on *Heller and Dickinson* [1985] and *Richards et al.* [1998].

volcaniclastics from the Klamath Mountains [*Heller and Ryberg*, 1983; *Heller et al.*, 1985]. Clockwise basin rotation of more than 50° has occurred since the middle Eocene [*Simpson and Cox*, 1977; *Wells and Heller*, 1988]. The OCR is currently undergoing east-west oriented compression due to ongoing subduction and forearc rotation and has been deformed into a series of gentle folds trending NE to SW with beds dipping 4 to 10° along fold flanks [*Baldwin*, 1961].

2.2. Rock Uplift and Erosion Rates in the Oregon Coast Range

The Oregon Coast Range has been proposed to approximate steady state [e.g., *Reneau and Dietrich*, 1991; *Montgomery*, 2001; *Roering et al.*, 2007] as numerous studies suggest that long-term erosion rates [e.g., *Bierman et al.*, 2001; *Heimsath et al.*, 2001] approximately balance rates of rock uplift [*Kelsey et al.*, 1994]. Long-term coastal uplift rates derived from shore platform surveys range from 0.05 to 0.03 mm yr^{-1} over the last 100 kyr [*Kelsey et al.*, 1994]. Millennial-scale OCR erosion rates, derived from cosmogenic nuclides, range from 0.03 to 0.3 mm yr^{-1} for hillslopes and from 0.11 to 0.14 mm yr^{-1} for basin-averaged erosion rates via stream sediments [*Bierman et al.*, 2001; *Heimsath et al.*, 2001]. *Reneau and Dietrich* [1991] analyzed colluvial hollows and estimated hillslope erosion rates of 0.07 mm yr^{-1} and bedrock exfoliation rates of 0.09 mm yr^{-1} over the last 4000 to 15,000 years. Short-term erosion rates derived from river sediment yields range from 0.07 to 0.19 mm yr^{-1} [*Wheatcroft and Sommerfield*, 2005]. Together, these findings suggest that the average lowering rate of approximately 0.1 mm yr^{-1} is broadly consistent with rock uplift rates across the Oregon Coast Range over 1000 year timescales. However, there is scant theory constraining how rock properties, which can present in a watershed as knickpoints [*Stock et al.*, 2005], rocky balds [e.g., *Aldrich*, 1972], or resistant cliffs [*Chan and Dott,* 1983], may modulate erosion rates.

2.3. Pacific Northwest Forearc Sedimentary Units—Diagenetic Processes, Products, and Rock Properties

Understanding controls on bedrock composition and mechanical behavior is critical for unraveling how anomalous landform patterns and dynamics emerge in the absence of climate and/or tectonic variations. Our observations and previous contributions [e.g., *Lovell and Rogers*, 1969; *Galloway*, 1974; *Heller et al.*, 1985; *Ryu and Niem*, 1999] suggest that the Tyee Basin source rock and subsequent diagenetic processes influence rock composition. As such, an examination of sedimentary architecture, burial history, and diagenesis will presumably enable us to characterize and predict bedrock exhumation patterns as well as implications for landscape evolution at the local and regional scale.

Sandy turbidite deposits sourced from immature volcaniclastic sediments along the Cascadia margin have been well studied for their characteristic diagenetic sequences [e.g., *Galloway*, 1974, 1979; *Ryu and Niem*, 1999]. Diagenetic alteration products are a function of the complex interplay between source minerals, depositional setting (e.g., shallow delta systems, submarine turbidity deposits on a continental shelf, or distal deepwater fan deposits), fluid flow, and burial depth [*Hutcheon*, 1983]. *Galloway* [1974, 1979] described three progressive stages of diagenesis based on shallow to moderate burial depth within the terrigenous and volcanic clastic deposits of the northeast Pacific arc-related basins. *Ryu and Niem* [1999] extended the diagenetic sequence to the Tyee forearc depositional system; the three progressive stages of diagenesis include the following: (1) calcite and calcite cement, (2) authogenic clay coats and rims, and (3) pore-filling zeolite cements (Figure 2). The authogenic clays include mixed layer chlorite/smectite (corrensite), which is compositionally related to palygorskite and sepiolite [*Weaver*, 2000], fibrous rimming clays mined industrially

for their binding strength [*Galan*, 1996]. While matrix-filling clays tend to reduce rock strength [*Al-Tahini et al.*, 2006], overgrowth (rimming) fibrous clays as we describe here often increase rock strength [*Yatsu*, 1971, 1988; *Al-Tahini et al.*, 2006].

2.4. Local Petrology, Mineralogy, and Depositional Setting

Previous petrology and mineralogy studies in the OCR noted the presence of rock strengthening or fibrous minerals in a zone extending from just north of Roseburg (latitude 43°) to Eugene, Oregon (latitude 44°), a region that roughly corresponds with the coarse-bedded slope and proximal ramp deposits of the Tyee [*Heller and Dickinson*, 1985]. Below, we consider the Pacific Northwest diagenetic phase model [*Galloway*, 1974, 1979; *Ryu and Niem*, 1999] in conjunction with several references describing patches of anomalous chlorite-calcite-rich, fibrous clays and resistant rock beds found in a 100 km swath in the southwest portion of the Tyee formation (Figure 1a, inset). Together, this information provides a regional context for diagenetically driven resistant bedrock in the OCR and allows us to constrain the spatial extent of potential morphologic and process effects.

Lovell and Rogers [1969] found no significant regional or local variation in the Tyee mineralogy with the exception of authogenic chlorite, but this does not preclude variations in minor secondary authogenic alteration products, oft noted but deemed unimportant to petrologic studies [e.g., *Lovell and Rogers*, 1969]. From a petrologist's point of view these are minor differences, while from a geomorphologist's point of view, the resulting difference within a single formation may be as profound as a difference in lithology in terms of controlling rock properties and thus geomorphic function. These diagenetic artifacts include chlorite and calcite, which grade with depth into later phases of authogenic calcite cements, rimming clays, clinoptiolite, and laumentite (Figure 2) [*Galloway*, 1974; *Chan*, 1985; *Ryu and Niem*, 1999].

Tyee samples collected to the west of Roseburg, Oregon, commonly have a chlorite matrix, and many have a radiating fibrous structure [*Rogers and Richardson*, 1964] suggestive of the rimming corrensite clays or the zeolite pore fill described by *Ryu and Niem* [1999]. Similarly, waterfall-forming Tyee sandstone beds in the South Coquille River (south of our study area) contain a fibrous authogenic mineral formed interstitially by the alteration of coarse volcanic grains [*Dott*, 1966]. In addition, calcite cemented beds occur locally [*Snavely et al.*, 1964; *Lovell*, 1969; *Lovell and Rogers*, 1969; *Stock and Dietrich*, 2006] in the "Smith River section" deposits. Carbonate concretions are found in 23% of the sandstone beds in the Smith River section [*Lovell*, 1969], which encompasses the watersheds that are the focus of this study. Nowhere else in the Tyee Formation is authogenic carbonate found in more than 4% of the beds sampled [*Lovell*, 1969]. Taken together, these studies suggest a well-defined zone for the resistant bed occurrence extending from 43°N to 44°N with a vertical extent limited by diagenetic phase zones (Figure 1a, inset). The extent of the resistant beds should migrate northward as deeper sections of the unit are exposed, tracking the delta submarine ramp deposition progression through time.

2.5. Geologic Structure and Resistant Beds in Franklin and Harvey Watersheds

In our central OCR study area, the Harvey and Franklin watersheds present an ideal opportunity to characterize the influence of variable rock properties, specifically rock strength, on landscape processes at the local (outcrop) to watershed scale, as meter-scale bands of diagenetically derived cliff-forming resistant rock, previously masked by surrounding dense vegetation, are now easily mapped using airborne lidar. The two watersheds occur within the Tyee Formation, are similarly orientated, and experience similar climatic and tectonic controls. Composed primarily of massive sandstone turbidite beds of variable thickness (ranging from ~1 to 10 m), with minimal siltstone inner beds, both Franklin and Harvey watershed stratigraphy exemplify turbidity deposits formed in the proximal region of a submarine ramp setting (Figure 2) [*Heller and Dickinson*, 1985]. Structurally, a broad (>1 km) anticline defines the region, with a minor fold axis trending N-NNE superimposed on the larger broad anticline. As the beds dip gently (~4–6°) away from the fold, resistant beds exposed in the Franklin Creek watershed have yet to be exhumed in the adjoining Harvey watershed to the west (Figure 1). Resistant cliff-forming rock beds ranging from a meter to tens of meters in thickness crop out in Franklin and extend into the eastern side of Harvey watershed. The beds are massive with a mean vertical fracture spacing of 12.9 ± 1.7 m (mean ± SE) compared to the mean vertical fracture spacing of 0.6 ± 0.02 m (mean ± SE) for the "typical" Tyee (Figures S1 and S2 in the supporting information). The beds are horizontally continuous but not contiguous. The resistant beds form knickpoints within the mainstem

channel of Franklin Creek and at varying elevations in tributaries. In general, resistant beds crop out at increasingly higher points in the drainage network moving from north to south (Figure 1).

3. Methods

3.1. Rock Properties: Petrographic and Mechanical Strength

To characterize rock properties in the resistant and typical sandstone, we collected in situ samples using a combination of sledges, rock hammers, and a diamond-bit corer. For petrographic analysis, we used thin sections for standard and polarized microscopy as well as SEM (scanning electron microscopy) for energy-dispersive X-ray spectrometry line scanning and 2-D mapping. We also infused all thin sections with blue epoxy to quantify variations in porosity. We estimated rock strength using two types of tensile failure tests, point load and Brazilian splitting tests. While both of these procedures measure tensile strength, the values differ depending on the testing procedure, and therefore the results are best interpreted as indexes of strength [*Butenuth*, 1997].

3.2. Topographic Characterization

3.2.1. Lidar Data and Topographic Noise

Our lidar-based topographic analysis of lithologic controls on landscape form used different methods to characterize topographic metrics depending on the process regime (e.g., hillslope versus valley) and scale. Our analysis of airborne lidar data (acquired by Oregon Department of Geology and Mineral Industries) required smoothing of the 1×1 m gridded bare earth data set. Noise in the bare earth data arises from two sources: (1) errors in point classification and (2) natural topographic roughness associated with tree throw pit and mounds, animal mounds, sediment piles, and large woody debris jams. In the OCR, the topographic signature of pit and mound features from tree turnover dominates at length scales < 7.5 m [*Roering et al.*, 2010]. Thus, for our calculations of hillslope gradient, curvature, drainage area, and relief, we smoothed the topography with a 2-D, second-order polynomial applied to a 10×10 m moving window [*Wood*, 1996; *Hurst et al.*, 2012].

3.2.2. Mapping Resistant Beds

From field observations on hillslopes and in channels, we consistently find that the resistant rock beds form cliff-like, vertical faces. Combining these field observations with airborne lidar data, we defined the resistant beds as having gradients equal to or greater than 1.0 (100%) based on smoothed slope values. This approach is similar to the method employed by *DiBiase et al.* [2012] and *Heimsath et al.* [2012]. Based on our field observations and field maps, this slope threshold successfully identified resistant beds throughout the Franklin Creek watershed (Figure 1).

3.2.3. Channel Network—Longitudinal Profiles and Slope-Area Plots

River profiles that deviate from a smooth, concave-up form can potentially provide insight into tectonic and lithologic controls on valley network processes [e.g., *Hack,* 1957; *Duvall et al.*, 2004; *Wobus et al.*, 2006; *DiBiase et al.*, 2010; *Kirby and Whipple*, 2012]. Channel slope is commonly quantified as a function of contributing drainage area described by a power law:

$$S = k_s A^{-\theta} \tag{1}$$

where S is the local channel slope; k_s, a dimensional constant, is the steepness index [$L^{2\theta}$]; A is the contributing drainage area [L^2]; and θ is the concavity index. Given steady state conditions, k_s is a function of rock uplift [*Snyder et al.*, 2000; *Wobus et al.*, 2006] as well as channel width, rock properties, climate, and sediment supply [*Howard*, 1998; *Whipple*, 2004; *Sklar and Dietrich*, 2006; *Ferrier et al.*, 2013]. Although a multitude of studies use k_s values to map relative variations in channel incision [e.g., *Wobus et al.*, 2006; *Kirby and Whipple*, 2012 and citations within], we used the same relationships to explore the role of resistant rock on channel profiles and channel processes [*Duvall et al.*, 2004; *Allen et al.*, 2013].

We followed standard network delineation procedures [*Wobus et al.*, 2006], choosing a threshold area of 5000 m^2 in order to extend the valley network above the fluvial network and into low-order, debris flow-prone portions of the valley network [*Lague and Davy*, 2003; *Stock and Dietrich*, 2006]. We calculated channel slope, drainage area, and the spatial integral of the drainage area versus elevation (chi plots) [*Perron and Royden*, 2013] using the Stream Profiler tool [*Whipple et al.*, 2007] with a 10 m smoothing length scale and a vertical sampling interval of 0.1 m to capture knickpoints and resistant bed forms in the channel. Because the

downstream portions of the channel network are alluvial, we restricted the slope-area plot fits to the bedrock portion of the channel network. Specifically in Harvey watershed the slope-area plots extend to an area ~3 km upstream from the river mouth, and in Franklin the plots extend to an area ~1 km upstream.

3.2.4. Valley Width

Valley width controls hyporheic exchange [*Kasahara and Wondzell*, 2003], sediment storage, and river features supporting aquatic function such as overwintering habitat during large flood events [e.g., *Naiman and Bilby*, 1998]. To measure valley width, we followed the methods employed by *May et al.* [2013], which entails using a slope gradient map derived from the smoothed lidar data set to identify valley floors from steep, adjoining hillslopes. We measured cross sections perpendicular to the valley axis on a hillshade map overlain with the gradient values along straight sections of stream reaches in the mainstem and tributary channels of Franklin Creek. For Harvey Creek, we used valley width data previously described in *May et al.* [2013]. We did not include valley width measurements in reaches with debris flow deposits as the aggraded sediment and large woody debris deposits are transient features that complicate interpretations of valley width.

3.3. Hillslope Gradient-Erosion Model

To estimate the extent to which resistant beds retard channel incision and regulate upstream erosion rates, we employed a theoretical model for the relationship between erosion and average hillslope gradient previously calibrated in the OCR. At low gradients, the relationship between slope and erosion rate is linear and then becomes highly nonlinear as slopes steepen to near critical values [e.g., *Montgomery and Brandon*, 2002]. In this nonlinear regime, small increases in erosion rates lead to rapid increases in sediment flux, such that hillslope gradients are not sensitive to erosion rate variations [*Roering et al.*, 1999; *Ouimet et al.*, 2009; *Dibiase et al.*, 2010]. Based on a one-dimensional, steady state solution, the functional relationship between dimensionless average hillslope gradient (R^*) and erosion rate (E^*) is given by *Roering et al.* [2007]:

$$R^* = \frac{S_h}{S_c} = \frac{1}{E^*}\left(\sqrt{1+(E^*)^2} - \ln\left(\frac{1}{2}\left(1+\sqrt{1+(E^*)^2}\right)\right) - 1\right) \tag{2}$$

where S_h is the average hillslope gradient and S_c is the critical slope gradient. The dimensionless erosion rate, E^*, is given by

$$E^* = \frac{2E\left(\frac{\rho_r}{\rho_s}\right)L_H}{KS_c} = \frac{2C_{HT}L_H}{S_c} \tag{3}$$

where E is the erosion rate (LT^{-1}); ρ_r and ρ_s are the rock and soil densities (ML^{-3}), respectively; L_H is the average hillslope length (L); C_{HT} is hilltop curvature (L^{-1}), defined here as the Laplacian of elevation (L^{-1}) [see *Roering et al.*, 1999; *Hurst et al.*, 2012]; and K is the soil transport coefficient (L^2T^{-1}) which incorporates factors such as the vigor of soil disturbances, soil properties, and climate. In Franklin Creek, we applied this model to soil-mantled hillslopes developed on the typical Tyee units that are perched above resistant bedrock cliffs and knickpoints. In doing so, we assumed that base level imposed by erosion of the resistant beds is reflected in the upstream hillslopes.

To determine the average hillslope length (L_H) in subcatchments of both Harvey and Franklin, we directly measured the horizontal distance from ridgetop to the valley centerline along the path of steepest descent following the methodology of *Hurst et al.* [2012]. In Franklin, we measured L_H in seven first-order basins; $L_H = 104.24 \pm 11.69$ m (mean ± SD). In Harvey watershed, we measured L_H in five first-order basins where $L_H = 73.01 \pm 8.98$ m (mean ± SD). For the remaining variables in equations (2) and (3), we used previously published values specific to the OCR [*Roering et al.*, 1999, 2007].

3.4. Hilltop Curvature-Erosion Model

On soil-mantled hilltops, erosion rate increases linearly with hilltop curvature according to

$$E = \frac{\rho_s}{\rho_r}KC_{HT} \tag{4}$$

We extracted curvature and gradient data from representative ridgetops throughout the Franklin and Harvey watersheds. In addition to the Harvey ridges in catchments H1 and H2, we sampled from the central and eastern portions of the watershed. In Franklin watershed, we extracted ridgetop data from study catchments F1–F4 and from a ridge in the southern portion of the watershed (Figure 1). Hilltops integrate erosion rates

imposed from adjoining valleys via the shared ridgetop. Thus, when selecting hilltops in Franklin watershed, we were careful to select hilltops for which resistant bedrock cliffs modulate both adjacent valleys. In both Harvey and Franklin, we selected hilltops with gradients <0.4, restricting our analysis to regions where curvature is proportional to erosion rates [*Roering et al.*, 1999], and extracted curvature values along five ridges with an average length of ~80 m.

3.5. Spectral Analysis—Biotic Signatures

We applied spectral analysis to quantify the extent to which resistant beds influence the biotic signature of tree rooting activity on the landscape. We hypothesize that the massive, soil-free, sandstone beds limit soil production due to their unfractured character. With a measured fracture spacing ranging from 10 to 25 m (12.9 ± 6.3 m, mean ± SD) in the resistant rock compared to closely spaced fractures ranging from 0.5 to 1 m (0.6 ± 0.2 m, mean ± SD) in the typical Tyee (Figures S1 and S2), we hypothesize that the lack of soil on the resistant beds may reflect resistance to tree root disturbance and turnover. To test whether resistant beds exhibit the characteristic topographic signature of tree turnover via pit and mound features, we used a 1-D spectral analysis of the raw gridded data over both soil-mantled typical Tyee areas and non-soil-mantled, resistant slope patches. We extracted topographic profiles of elevation along horizontal hillslope transects from unsmoothed gridded lidar data in areas where the raw lidar point cloud data exhibits a high density of bare earth returns for both soil-mantled ($n = 3$) and resistant rock ($n = 3$) swaths. We then interpolated the profile data to a 1 m spacing and applied a 1-D discrete Fourier transform (1-D DFT). Fourier spectral analyses transform discrete information from the spatial domain into the frequency domain, which quantifies how the amplitude of topographic features (such as tree disturbances or mima mounds) are distributed across a range of spatial frequencies or wavelengths [*Rayner*, 1972; *Hanley*, 1977; *Harrison and Lo*, 1996; *Perron et al.*, 2008]. The DFT of a one-dimensional data set, $z(x)$, consisting of N_x measurements at equal intervals of Δx, can be written as

$$Z(k_x) = \sum_{m=0}^{N_x-1} z(m\Delta x) e^{-2\pi i\left(\frac{k_x m}{N_x}\right)} \tag{5}$$

where k_x is wavenumber and m is the index in z [*Priestley,* 1981].

To estimate the power spectrum of z, we used a DFT periodgram, which provides a measure of how the variance of z varies with the frequency. One common way of estimating the power spectrum is

$$V_{\mathrm{DFT}} = \frac{1}{N_x^2} |Z(k_x)|^2 \tag{6}$$

where V_{DFT} equals the variance with the units of amplitude squared. Parseval's theorem states that because the Fourier transform is unitary, the sum of the power spectrum is equal to the variance of z. In order to compare spectra variance between the resistant and typical rock, we normalized the profiles to have a total variance of 1 (m^2).

3.6. Topographic Relief

The length scale for calculating topographic relief is often determined a priori by using an ad hoc radius in order to describe elevation differences within a drainage basin [e.g., *Ahnert*, 1987; *Montgomery and Brandon*, 2002]. At the hillslope scale (100 m radius), relief is strongly correlated with mean basin gradients, while at larger window sizes, the steepness of tributaries (1–5 km), major rivers (>10 km), and range height is incorporated into the relief metrics [*Whipple et al.*, 1999; *DiBiase et al.*, 2010]. We performed an analysis of dominant length scales in Franklin and Harvey watersheds to determine whether pervasive resistant beds in Franklin could alter the competition between diffusive and advective processes and therefore valley ridge spacing [*Perron et al.*, 2009]. We measured ridge-valley spacing at both the hillslope scale and the larger catchment scale (e.g., catchments F1–4 and H1–2, Figure 1) in ArcMap, recording 50 ridge-to-ridge lengths at both the unchanneled and major ridge-valley scales in Franklin and Harvey for a total of 200 measurements. Given the generally ovoid catchment shapes, we chose the mean width when measuring ridge-to-ridge lengths.

4. Results

4.1. Petrology and Tensile Strength

From thin section analysis, we found no significant difference in grain size, porosity, or mineral composition between the typical ($n = 5$) and resistant ($n = 9$) Tyee rock samples. All samples contain angular micaceous

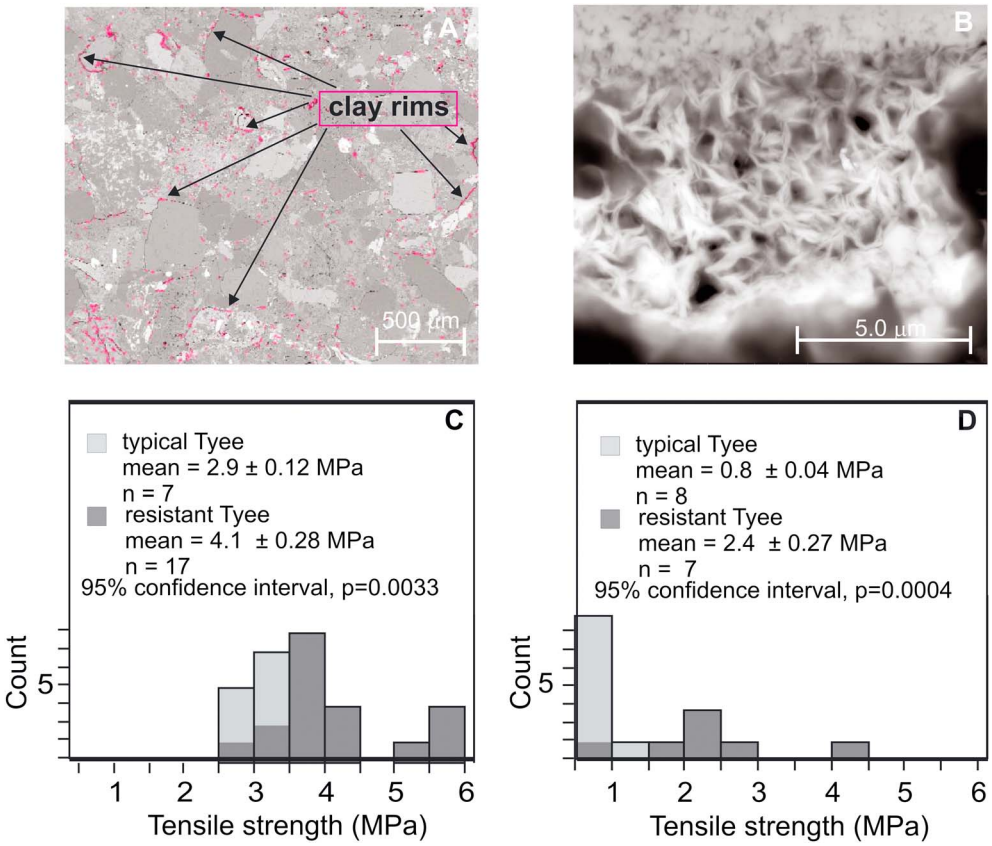

Figure 3. (a) Backscatter scanning electron (BSE) microscope image of resistant rock. Black arrows point to diagenetic clay rims. (b) Close-up of fibrous rimming clay. Crystalline feature at the top and bottom of the BSE image are mineral grains cemented by the fibrous clays. (c and d) Stacked histograms of rock tensile strengths for typical and resistant rock calculated from load measurements using a using a point load device (Figure 3c) and the Brazilian splitting test (Figure 3d). Reported values are mean ± standard error.

arksoic grains and immature volcanic clastics within patches of pseudomatrix. We observed no calcite or calcite cement in the typical or resistant rock, although chlorite and chlorite cement appears sporadically in resistant rock samples. A distinct difference between the resistant and typical samples is the very minor (<1%) amounts of diagenetic rimming clay in the resistant rock. The rimming clay is fibrous and forms an intergrain framework (Figure 3). Qualitative elemental analysis using the SEM energy-dispersive X-ray spectrometry function suggests that the rimming clays are from a class of mixed layer clays that includes corrensite, heulandite/clinoptilolite, and laumonite, any one of a group of fibrous clays that have been shown to cement and strengthen rock [*Ryu and Niem*, 1999; *Al-Tahini et al.*, 2006]. These mixed layer clays are found in turbidite detrital deposits [*Callen*, 1984] and are closely related to clays used as industrial binders [*Galan*, 1996].

Tensile strength tests using a point load device and a Universal Testing Machine (Brazilian splitting test) reveal significant differences in rock strength. We ran two sets of tests, the first using a point load device on 25–28 mm diameter, 11–14 mm length cores of typical Tyee ($n = 7$) and resistant Tyee ($n = 17$) and the second using the Universal Testing Machine on 50–51 mm diameter, 25–39 mm length cores on typical Tyee ($n = 9$) and resistant Tyee ($n = 6$). Average tensile strengths using the point load device are 2.94 ± 0.12 MPa for the typical Tyee and 4.10 ± 0.28 MPa for the resistant samples. Using the Universal Testing Machine, we also observe a significant difference in tensile strengths, with the tensile strength for typical samples equal to 0.83 ± 0.04 MPa compared to 2.06 ± 0.27 MPa for resistant samples (Figure 3). (All values are mean ± SE.) The patchy nature of the diagenetic artifacts within the resistant rock samples likely results in the observed variability in tensile strength. The differences between the tensile strength mean values for the two sample populations are significant at the 99.6% and 99.9% levels for the point loading and Brazilian splitting tests, respectively. Because the Brazilian splitting test is more common for geomorphic investigations such as bedrock valley erodobility [e.g., *Sklar and Dietrich*, 2001; *Stock et al.*, 2005] and, more importantly, produces

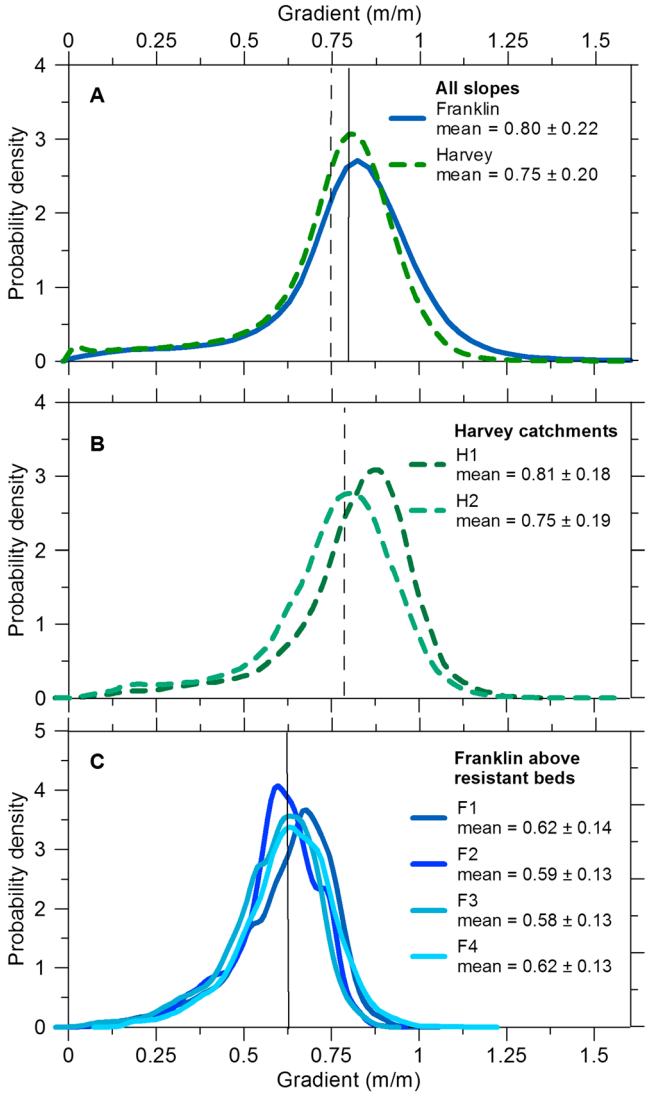

Figure 4. Hillslope gradient probability density functions (PDFs) with means and standard deviations for (a) Franklin and Harvey watersheds, (b) Harvey catchments H1 and H2, and (c) Franklin subcatchments F1–F4, above resistant rock beds. Solid lines and dashed lines refer to Franklin and Harvey PDFs, respectively.

valid results over the greatest range of rock strengths [*Vutukuri et al.*, 1974; *Sklar and Dietrich*, 2001], we favor the mean values of 0.83 MPa for the typical and 2.06 MPa for the resistant Tyee samples.

4.2. Rock Controls on Catchment Morphology

4.2.1. Hillslope Gradients

Visual inspection of airborne lidar for the two watersheds reveals remarkably consistent topography in Harvey watershed—with evenly spaced ridges and valleys and sharp and convex ridgetops giving way to planar hillslopes. By contrast, Franklin Creek is characterized by much less consistent ridge-valley spacing and, importantly, perched, gentle soil-mantled valleys above resistant, steep bedrock outcrops (Figure 1). We calculated the fraction of resistant beds in each watershed and found that 12% of Franklin topography compared to $<4\%$ of Harvey is composed of resistant beds. Furthermore, the resistant beds in Harvey crop out in a patchy and dispersed fashion along the eastern margin of the catchment, which contrasts with abundant, spatially extensive resistant beds in Franklin. To determine if catchment-average morphologic metrics such as average hillslope angles reflect the influence of resistant rock beds, we calculated the distribution of hillslope gradient in both Harvey and Franklin watersheds (Figure 4). (All reported mean gradient values include the mean ± SD.) Hillslope gradient distributions do not reveal a statistical difference between the two watersheds as the mean hillslope gradient in Franklin watershed is 0.80 ± 0.22, while the mean hillslope gradient in Harvey watershed is 0.75 ± 0.20 (Figure 4). The similarity in hillslope gradient distributions exists despite a nearly threefold difference in the proportion of resistant beds in Franklin compared to Harvey watershed.

We performed a similar hillslope gradient analysis focusing on small tributaries within both of our study catchments. Specifically, we targeted small catchments perched above resistant beds in Franklin Creek (Figure 1) and identified catchments of similar size in Harvey Creek for comparison. In contrast to the indistinguishable catchment-averaged slope distributions, small tributary hillslope gradients vary significantly depending on the presence or absence of the resistant rock. Two of the Harvey subwatersheds with uniform ridge-valley spacing (H1 and H2) gradients are statistically indistinguishable from each other and from the mean Harvey watershed hillslope gradient (Figure 4). The mean hillslope gradient for H1 is 0.81 ± 0.18, and for H2 is 0.75 ± 0.19. By contrast, the gradient distributions for the Franklin tributaries show consistently lower values of average gradient, with means of 0.62 ± 0.14 (F1), 0.59 ± 0.13 (F2), 0.58 ± 0.13 (F3), and 0.62 ± 0.13 (F4). Taken together, these results suggest that the resistant beds increase the variance of hillslope gradient.

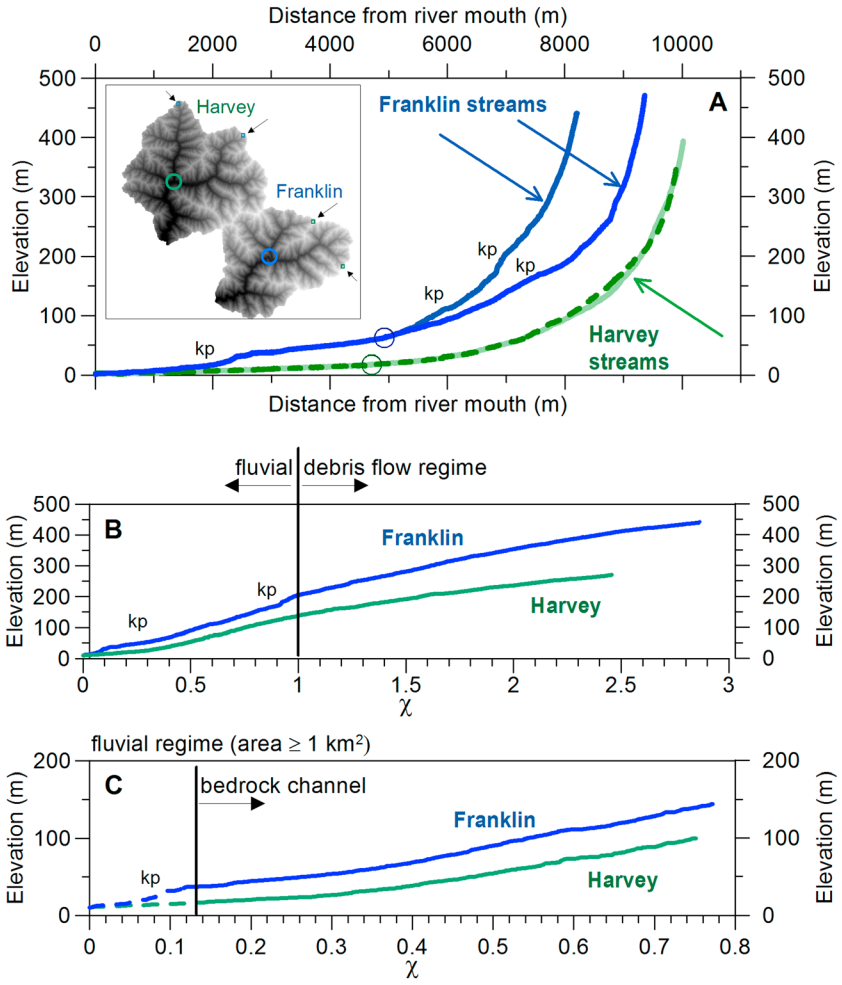

Figure 5. (a) Longitudinal profiles extracted from Franklin and Harvey watersheds. Arrows on inset DEM identify the starting location for each of the four drainages plotted. Open circles on DEM and profiles delineate where drainages merge. We identify knickpoint locations with "kp." (b) Elevation versus the spatial integration of drainage area comparing data from two of the four drainages plotted in Figure 5a. We plot data for valleys and channels with drainage area $>$ 0.05 km2. (c) χ plots as in above, plotted for just the fluvial portion of the drainage network defined as drainage area $>$ 1 km^2. Dashed lines identify the alluvial portions of the network. For all χ plots we use a concavity value of -0.56.

4.2.2. Influence of Resistant Beds on Channel and Valley Network Form

To explore the influence of the resistant beds on valley slope, we plotted longitudinal channel profiles for Franklin and Harvey watersheds as well as longitudinal profiles for individual subwatersheds within the two larger basins (Figure 5a, inset map). The longitudinal profiles in Harvey exhibit smoothly varying, concave upward forms and show remarkable consistency. In contrast, Franklin watershed profiles show a significant knickpoint approximately 2000 m upstream from the river mouth with a plethora of smaller knickpoints apparent further upstream (Figure 5a). In addition, we employed chi (χ) plots to examine the apparent elevation difference between the watershed longitudinal profiles. Chi plots linearize slope drainage area data by expressing the spatial integral of the drainage area against elevation [*Whipple et al.*, 2007; *Perron and Royden*, 2013]. Chi plots are only truly linear if erosion is steady and concavity and steepness are constant along the length of the analysis [*Willett et al.*, 2014]. The plots are beneficial for their ability to reduce noise common to slope-area data sets and to identify transitions in processes controlling channel form [*Mudd et al.*, 2014]. To compare the watersheds, we used the Harvey watershed longitudinal concavity value of -0.56, which reflects the fluvial bedrock portion of the networks (Figure 6). We first plot elevation against χ for the length of the entire valley network (Figure 5b), including both the debris flow and fluvial regimes. We observe an inflection in the chi plot that appears to correspond with the process transition between fluvial and debris

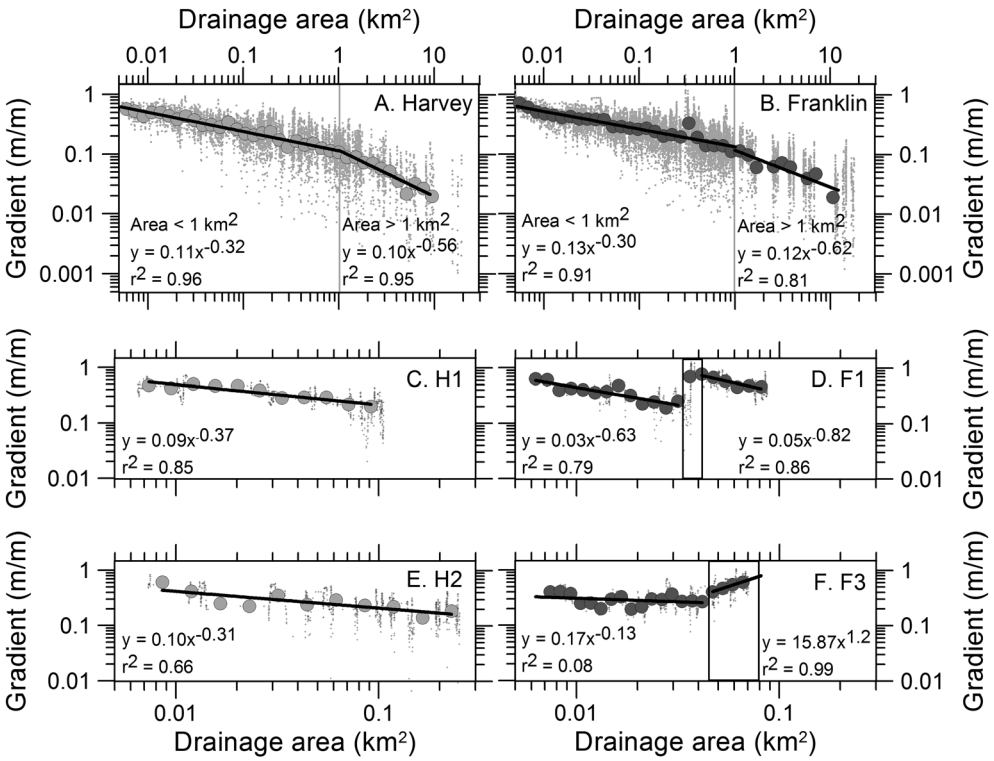

Figure 6. Slope drainage area plots for (a) Harvey and (b) Franklin watersheds and subwatersheds (c) H1 and (e) H2, and (d) F1 and (f) F3. Rectangles delineate location of resistant beds within Franklin catchment plots. We plot raw slope-area data with small markers. To minimize raw data noise, we log-bin the data by equal drainage area width (large circle markers) and fit regressions to the log-binned data. Bins for the alluvial sections are not included.

flow regimes. This transition corresponds with the 1 km slope-area scaling break representing the transition between debris flow and fluvial regimes (see below and *Stock and Dietrich* [2003]). To explore elevation differences in the fluvial portion of the channel network, we display the lower portion of the channel network at drainage areas ≥ 1 km^2 (Figure 5c). For the Franklin watershed, the χ plot exhibits a steeper slope and is offset relative to the Harvey data (Figures 5b and 5c) likely reflecting the ability of resistant bedrock beds to support the Franklin catchment at higher elevations. As the χ plot slope above the knickpoints in Franklin continues to steepen relative to Harvey, we interpret the systematic χ-elevation difference as a reflection of base level modulation by resistant beds limiting incision upstream.

Slope-area plots reflect process domains such as the transition between debris flow and fluvial valleys [e.g., *Montgomery and Foufoula-Georgiou*, 1993; *Stock and Dietrich*, 2003] and incision rates as inferred from steepness indexes [e.g., *Snyder et al.*, 2000; *Kirby and Whipple*, 2001, 2012]. In both Franklin and Harvey watersheds, we qualitatively observe a scaling break at drainage areas ~1 km^2 and slopes of 0.1, which likely represents the transition between debris flow and fluvial valley carving processes in the Oregon Coast Range (Figure 6) [*Dietrich et al.*, 2003; *Stock and Dietrich*, 2003]. The slope-area plots for Franklin and Harvey are remarkably similar, especially for drainage areas < 1 km^2 despite the prevalence of resistant rock beds and hanging valleys in the Franklin watershed. The k_s (steepness) values for the fluvial portions of Harvey and Franklin are 0.11 and 0.13, respectively, while θ (concavity) values are -0.56 and -0.59, respectively. These concavity estimates are consistent with values previously measured in the central and southern OCR [*Seidl and Dietrich*, 1992; *Kobor and Roering*, 2004; *VanLaningham*, 2006]. While we still lack a complete understanding of the functional relationship between slope and area in debris flow regimes [e.g., *Stock et al.*, 2005], we can qualitatively assess differences in Harvey and Franklin debris flow slope-area plots. Similar to our hillslope gradient results, slope-area plots for individual subwatersheds again correspond closely in Harvey watershed and exhibit variability in the Franklin watershed. Slope-area plots for Harvey watersheds H1 and H2 are nearly indistinguishable. In Franklin watershed, however, slope-area plots for watersheds perched above the resistant beds exhibit significant variability and differ from those observed in Harvey. Most importantly, Franklin

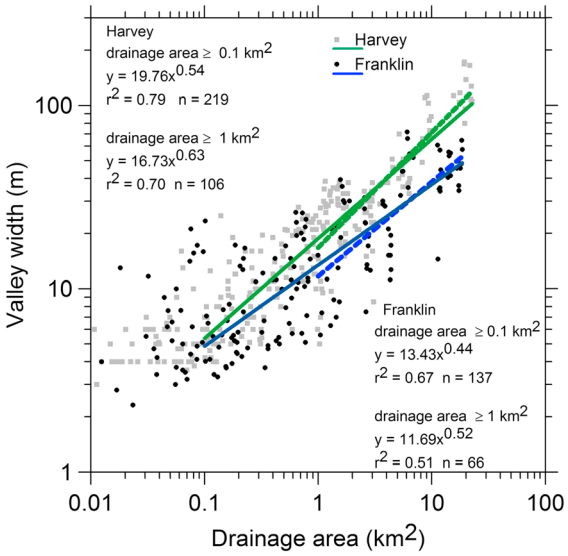

Figure 7. Valley width versus drainage area values extracted from lidar data for Franklin and Harvey watersheds. We fit power laws to drainage areas > 0.1 km^2 [following *May et al.*, 2013] and to drainage areas in the > 1 km^2 fluvial domain.

tributaries show an offset in slope-area data that separates terrain above the resistant beds from lower sections of catchments below resistant beds (Figures 6d and 6f). In F3, the resistant rock beds occupy a small fraction of the watershed and the downstream portion of the slope-area plot encompasses a band of resistant rock beds. In this case (F3), the θ value is positive (or convex), reflecting the strong influence of resistant bedrock on profile form.

As hillslope-channel interactions (e.g., lateral channel migration into hillslopes or channel avulsion due to landslides) influence valley morphology, we characterized the relationship between drainage area and valley width across for all basin orders in Franklin and Harvey watersheds (Figure 7). Following *May et al.* [2013], we focused on trends for drainage areas > 0.1 km^2. We observe a power law relation between drainage area and valley width for both watersheds (Figure 7), and this relationship is robust when restricting the analysis to the fluvial domain (areas > 1 km^2). In essence, valley width increases more rapidly with drainage area in Harvey than in Franklin and this difference is significant at the 99% level. In Franklin watershed, we also observe greater variability in valley width with drainage area, likely reflecting the influence of the resistant beds [*Allen et al.*, 2013].

4.2.3. Hillslope Model Predictions of Erosion Rate

For the hillslope gradient-erosion model, we used equations (2) and (3) with previously calibrated transport model parameters [*Reneau and Dietrich*, 1991; *Roering et al.*, 1999]: $K = 0.004$ m^2 yr^{-1}, $S_c = 1.25$, and $\rho_r/\rho_s = 2.0$, to generate erosion rate estimates for subcatchments in Harvey and Franklin. These equations apply to soil-mantled hillslopes that occur in areas that lack or are perched above the resistant beds. Analysis of smoothed lidar data indicates that hillslopes in Harvey watersheds are 1.3 times steeper than hillslopes above the resistant rock beds in Franklin (section 4.2.1 and Figure 4). For these small watersheds in Harvey and Franklin, we used mean hillslope gradient values (S_h) of 0.75 and 0.60, respectively; calculated corresponding R^* values of 0.6 and 0.48, respectively; iteratively solved equation (2) for E^*; and then used the first half of equation (3) to calculate E. In Harvey, the predicted erosion rate is 0.087 ± 0.19 mm yr^{-1} (mean and SE). By contrast, for Franklin hillslopes above the resistant rock beds, the calculated erosion rate is 0.037 ± 0.18 mm yr^{-1}, less than half the calculated erosion rate estimated in the Harvey watershed. To apply the hilltop curvature-erosion model, we estimated the mean hilltop curvature in Harvey watershed as -0.097 ± 0.015 m^{-1} (mean $\pm$ SD). The corresponding value for Franklin ridgetops is -0.053 ± 0.008 m^{-1} (mean $\pm$ SD), implying a nearly twofold difference in erosion rates (equation (4)) which is consistent with the hillslope gradient model result. From equation (4), hilltop erosion in Harvey watershed is calculated as 0.19 ± 0.012 mm yr^{-1} (mean $\pm$ SE), while the corresponding value in Franklin is 0.10 ± 0.016 mm yr^{-1} (mean $\pm$ SE).

We solved for E^* using the second half of equation (3) to explore how well R^* and E^* values for Franklin and Harvey compare with the nonlinear, dimensionless steady state denudation curve (equations (2) and (3) and Figure 8). In essence, this calculation determines the extent to which landform properties (in this case slope, curvature, and slope length) are consistent with steady state erosion given a previously calibrated set of process parameters (e.g., K, S_c). A key caveat of this analysis is that it combines a 1-D model prediction of hillslope gradient with a 2-D estimate of hilltop curvature. Nonetheless, R^*-E^* plots have been successfully used to assess erosion and hillslope adjustment in response to uplift and identify associated time lags in landscape response [*Hurst et al.*, 2013a]. Calculated E^* values for Franklin and Harvey are 3.05 and 5.1, respectively, with corresponding calculated R^* values of 0.48 and 0.6 generated from $R^* = S_h/S_c$. The Franklin

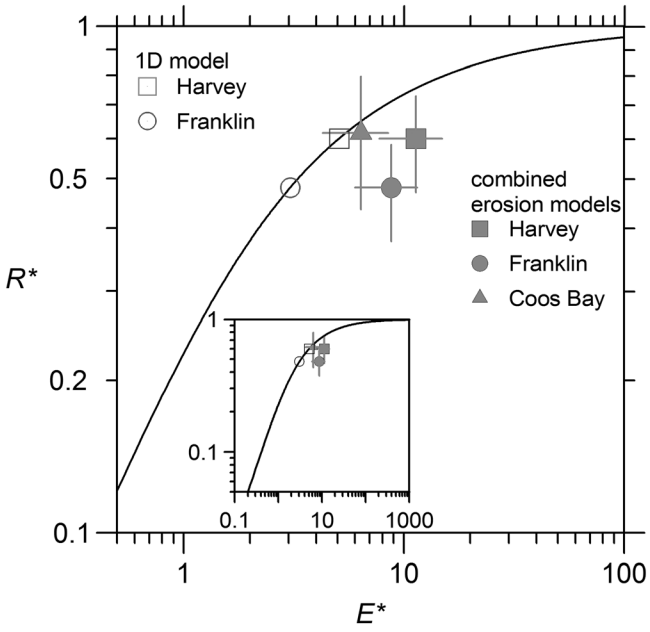

Figure 8. Functional relationship between dimensionless relief (R^*) and erosion rate (E^*). One-dimensional gradient-erosion model results plotted with open symbols (equation (2)). Combined 1-D and 2-D gradient-curvature-erosion model plotted with filled symbols (equations (2) and (3)) (see section 4.2.3). Inset plot displays expanded domain of the R^* versus E^* formulation. Note that the Franklin 1-D-2-D data point falls well below the steady state curve, perhaps reflecting a transient condition.

$R^* - E^*$ value is significantly offset from the steady state curve, and its position indicates lower than predicted relief (or faster than predicted erosion), while the Harvey is sufficiently close to the model curve such that steady erosion cannot be rejected (Figure 8). The offset Franklin $R^* - E^*$ values may reflect transient adjustment of the hillslopes above the resistant beds. Consistent with this interpretation, hillslope lengths for the Franklin catchments are >25% longer than those observed in Harvey, which may result from changes in the scale of landscape dissection associated with a slower base level lowering rate.

4.3. The Topographic Signature of Biotic Versus Abiotic Weathering

To determine whether cliff-forming, resistant beds are resilient to biotic weathering via tree root disturbances, we analyzed the roughness of topographic profiles. Most fractures in the Tyee Formation are vertical to subvertical, dissecting the horizontal beds. Average fracture spacing in the typical Tyee is less than 1 m, in contrast to the high average fracture spacing of 12.9 m in the resistant Tyee (Figure S2). Horizontal contacts between turbidite beds in the typical Tyee is usually <1 m, facilitating detachment by tree roots or burrowing animals. The resistant rock beds lack the topographic signature of pit and mound landforms that dominate the form of soil-mantled hillslopes (Figure 9). Specifically, the soil-mantled profiles generated atop typical bedrock slopes have higher spectral power at low (2 to 10 m) wavelengths compared to the resistant, bedrock profiles. In addition, the strong contrast in spectral slopes reflects the relative importance of different wavelength features in contributing to the total variance. Furthermore, the resistant rock spectra slope steepens at wavelengths of ~10 m, which corresponds to the fracture spacing obtained from field observations (Figures S1 and S2). In the typical Tyee profiles, high spectral power at low wavelengths likely incorporates the influence of submeter fracture spacing overprinted by biotic processes such as tree throw [*Roering et al*., 2010].

4.4. Resistant Beds and Relief

To identify the dominant scales of dissection in our study catchments, we measured ridge-valley spacing at both the smallest hillslope scale and at the scale of major ridge-valley sequences. In Franklin and Harvey, the hillslope spacing is essentially indistinguishable with mean lengths of 95 ± 4 m in Franklin (median = 88 m) and 97 ± 3 m in Harvey (median = 95 m) (mean ± SE). In Harvey, we also observe a tight cluster of length scales for the major ridge-valley sequences with a mean of 351 ± 11 m and a median of 345 m. In Franklin, the major ridge-valley spacing has a mean of 335 ± 21 m (median = 311 m). While the length scale is similar for both watersheds, Franklin values exhibit much greater dispersion, likely due to the prevalence of hanging valleys, cliff-dominated hillslope segments, and variable valley orientations. These results provide a length scale upon which to establish our local relief calculations.

Estimating topographic relief, here defined as the elevation range within a given area, enables us to evaluate how resistant rock beds influence landscape form at different scales in Franklin Creek. At the subwatershed scale, resistant beds control base level for first- and second-order catchments perched above the cliff-forming units. The location of the resistant beds within the catchment will likely dictate their effect on landscape morphology. We calculated relief in both watersheds using two radius values, 100 m and 350 m, as

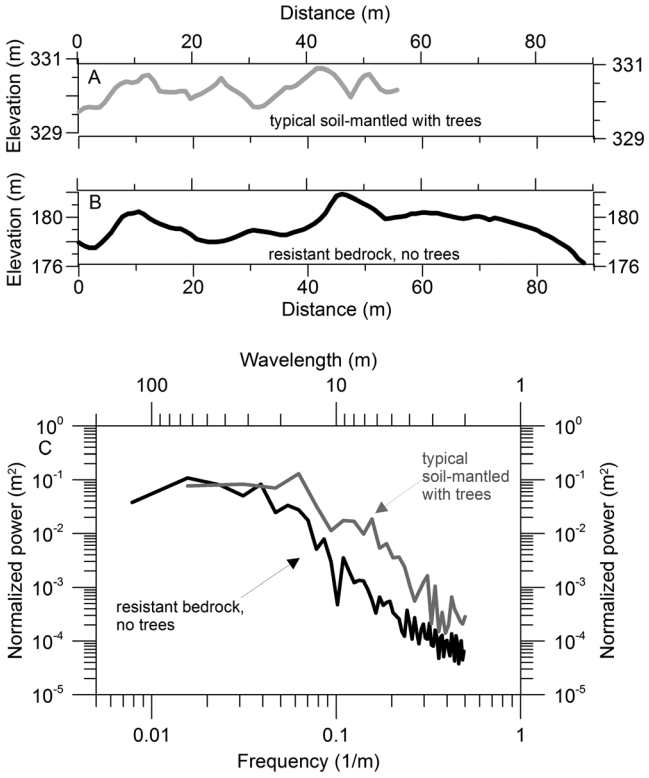

Figure 9. Topographic profiles of (a) soil-mantled and (b) resistant rock extracted along contour horizontal profiles from the unsmoothed gridded lidar data in Harvey and Franklin watersheds, respectively. (c) Averaged one-dimensional power spectra for soil-mantled ($n = 3$) and resistant rock ($n = 3$) profiles. Soil-mantled power spectra exhibit higher spectral power at wavelengths of 7 m and less. Resistant rock power spectra steepens at 10 m.

determined through our ridge-valley spacing analysis. At the 100 m scale, the mean relief in Franklin is 128 ± 22 m (mean ± SD), which is quite similar to the Harvey value of 116 ± 20 m (Figure 10a). At the 350 m scale, however, relief values are higher in the Franklin watershed compared to Harvey, and the topography exhibits a distinct decrease in relief moving SE to NW along the axis of the minor anticline that bisects Franklin Creek (Figure 10b). In Franklin, the 350 m radius relief values locally exceed 400 m, while Harvey values never exceed 345 m (Figure 10a). High relief zones in Franklin coincide with a high density of resistant rock beds, in the cliffs to the south along the Umpqua River, and along cliffs to the north (Figure 10b). Although resistant beds outcrop in Franklin due to an anticline [*Baldwin*, 1961], we suggest that the resistant beds control relief rather than the anticlinal structure, as we do not see elevated relief along other OCR anticlines in the typical Tyee. Additionally, we note regions with resistant rock and high relief values occurring away from the Franklin anticline (Figure 10b).

In order to quantify the potential relationship between resistant rock beds and local relief at the subcatchment and whole-watershed scale, we calculated the percentage of resistant rock beds (gradient ≥ 1) over 100 m and 350 m radii using a neighborhood function and compared those values to the average relief within that same window. We

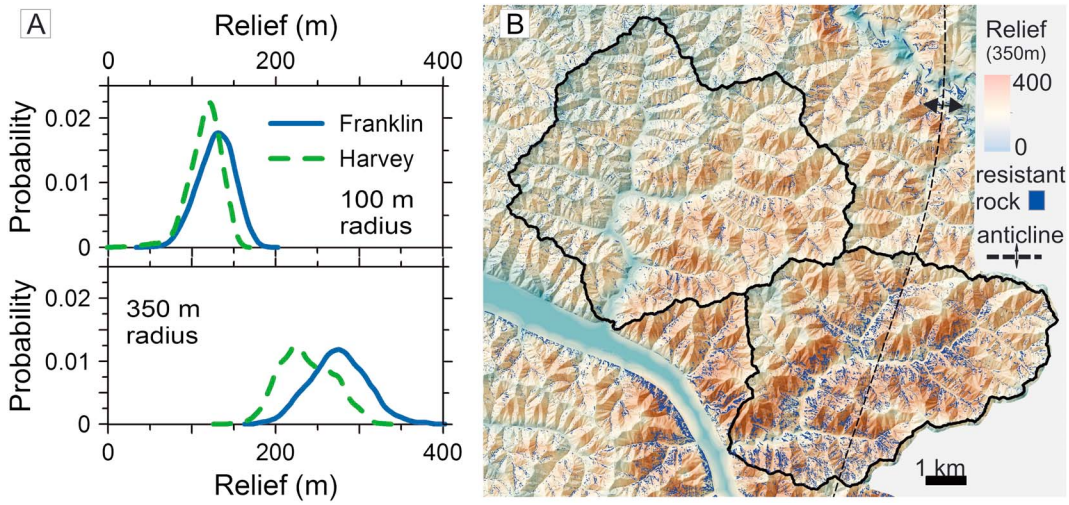

Figure 10. (a) Probability density functions for mean-local relief in Franklin and Harvey watersheds at (top) 100 m and (bottom) 350 m scales. (b) Relief values calculated over a 350 m radius. Areas with low relief are delineated by light blue tones, while high relief areas are shaded reddish-brown. We identify slopes with gradients ≥1 with dark blue coloration.

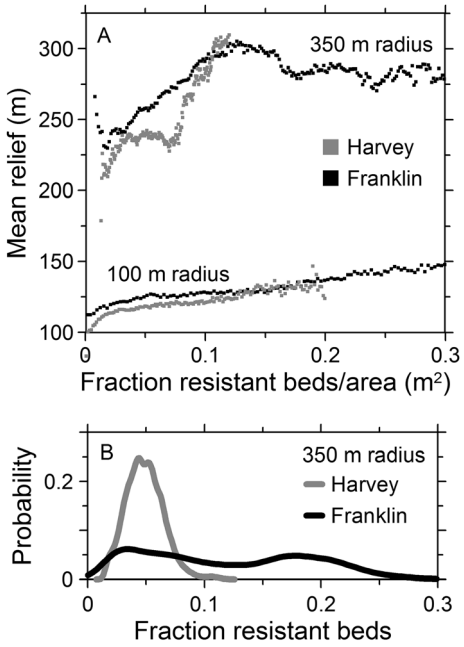

Figure 11. (a) Comparison of mean relief over 100 m^2 area and 350 m^2 area versus the fraction of resistant beds within each analytical radius. Length scales correspond to subcatchment and larger ridge-valley spacing. (b) Normalized distributions (PDFs) of percent resistant beds found within 350 m^2 area for each grid value. For all plots we generated a random subset of 64,000 samples for Franklin and Harvey watershed from data sets of 18 and 22 million points for Franklin and Harvey watersheds, respectively. In Figure 10a we binned the subsampled data into 100 evenly spaced bins.

condensed the large data sets generated from Franklin ($n > 18 \times 10^6$) and Harvey ($n > 22 \times 10^6$) into bins of equal percent width after extracting random subsets of 64,000 data points from each larger data set. For the 100 m analysis, the Franklin watershed has regions where the resistant beds comprise over 30% of the topography, while the Harvey watershed seldom exceeds 15% resistant beds. Not surprisingly, there is a strong correlation between mean relief and the percent of land with slope gradient ≥ 1.0 in both the Franklin and Harvey watersheds, as relief is similarly affected by local resistant bedrock at short length scales (Figure 11a, lower plot).

By contrast, the 350 m scale analysis reveals distinct differences in how resistant bedrock influences relief. While resistant rock beds appear in both Franklin and Harvey, there are very few continuous outcrops extending over length scales exceeding 100 m in Harvey. Only in Franklin watershed are the beds prevalent over continuous length scales coincident with the larger ridge and valley length scale. This is well illustrated in Figure 11b, which shows the fraction of resistant rock beds within a 350 m radius for both Franklin and Harvey watersheds. In Harvey, resistant beds never compose more than 12% of the topography within a 350 m radius and rather have a mean density of ~5%. This contrasts with Franklin where the resistant rock beds account for 0 to 30% within a 350 m radius (Figure 11b). We observe a positive monotonic relationship between percent resistant beds and relief in Franklin that levels off when the local density of resistant beds exceeds 15%. At greater percentages the relationship breaks down, which is consistent with the declining density of resistant bedrock at percentages > 18% (Figure 11a, top plot). In Harvey, local relief at the 350 m scale does not increase with the density of resistant beds, likely reflecting the patchy, discontinuous nature of the resistant beds in that watershed.

5. Discussion

Geomorphologists frequently list the triumvirate of lithology, climate, and tectonics when describing the fundamental controls on landscape evolution. In this study, we ask the following question: What is the geomorphic significance of lithologic variation within a seemingly uniform geologic unit? Geomorphologists commonly cite uniform rock type and proceed to ascribe topographic patterns to tectonic, climate, or geomorphic process differences. In the well-studied Oregon Coast Range, lidar allows us to confront the geomorphic implications of lithologic variability. Our analysis indicates that diagenetic variations in rock properties may influence a broad array of geomorphic processes and thus landscape form and evolution.

5.1. Sink to Source—Diagenesis to Rock Hardness

Our observations suggest that a diagenetic set of authigenic minerals and clay cements strengthen units that crop out as cliff-forming beds in Franklin Creek. These Eocene basin (sink) morphology-driven grain-scale reinforcements appear to be responsible for increasing tensile strength by 2.5 times relative to beds of the typical Tyee Formation (Figure 3). In turn, these present-day source materials influence modern hillslope and channel processes.

In this contribution, we do not pinpoint the exact mineralogical change associated with the diagenetic setting, given that the diagenetic processes in immature volcanic clastic sedimentary deposits allow for multiple clay minerals or cements with the potential to increase rock strength. However, our enhanced

understanding of the petrology, diagenetic processes, and artifacts shaping the Tyee improves our ability to calibrate model parameters and predict the extent of rock property influence on geomorphic function. Based on thin section and SEM analyses and an extensive review of the existing literature [e.g., *Rogers and Richardson*, 1964; *Snavely et al.*, 1964; *Lovell*, 1969; *Lovell and Rogers*, 1969; *Ryu and Niem*, 1999], our observations suggest that while calcite and chlorite cements are present throughout the sand-dominated, coarse-grained slope and proximal ramp deposits of the ancestral Tyee Formation (Figure 2), fibrous clays and/or abundant amounts of chlorite cement are distinct to the resistant beds. Our findings are corroborated by earlier observations of resistant Tyee beds in a region bounded as far south as the Coquille River and to the north by the Siuslaw river watershed [*Dott*, 1966; *Lovell*, 1969; *Chan and Dott,* 1983].

The horizontal and vertical spacing of the resistant beds in Franklin Creek is nonsystematic, and it is unclear whether climate, depositional patterns, diagenetic processes, provenance, or autogenic variability controls the bed spacing and thus the spatial and temporal influence of resistant beds on OCR landscape morphology. While speculative, we next ponder potential controls on the horizontal and vertical extent of the resistant beds. Postinitiation of the Cascadia subduction zone at 49 Ma, massive and prolific sediment inputs inundated the ancestral Tyee River along the fore arc [*Heller et al.*, 1987; *Dumitru et al.*, 2012]. Unconfined sheet flow down the delta slope dominated sediment transport to the basin plane, leading to little or no differentiation of the ramp slope into features such as deep canyons, overbank deposits, or interchannel areas [*Heller and Dickinson*, 1985]. Rather, the deposits formed as sheets of sediment distributed over the narrow continental shelf. The source river sediments were extremely well mixed [*Heller et al.*, 1992] with sediment accumulation rates greater than 0.7 mm yr^{-1} [*Chan and Dott*, 1983]. The horizontal continuous yet noncontiguous nature of the resistant rock within our study area may reflect a spatial limit to the individual packets of turbidite deposits flowing down a continental ramp (Figures 1, 2, and S1). Indeed, a survey of present-day bathymetric images in submarine ramp settings reveals a crenulated morphology reminiscent of the horizontal organization of the resistant beds in Franklin Creek. In addition to the noncontiguous horizontal spacing, vertical spacing of the resistant beds is also nonuniform, consistent with the variable bedding thickness in the Tyee Formation [*Heller and Dickinson*, 1985]. Using measured bed thicknesses ranging between 1 and 15 m in height and an average sedimentation rate of 0.7 mm yr^{-1} [*Chan and Dott*, 1983], we calculated that resistant bed deposition occurred over ~20 kyr intervals, which eliminates mechanisms including landslide deposits from deep subduction zone earthquakes, eustatic changes in sea level, or climate variability during the Eocene. Instead, the resistant rock beds may result from a combination of necessary and sufficient mineral assemblages derived from mafic contributions from the proto-Cascade arc at shallow burial depths [*Galloway*, 1974; *Ryu and Niem*, 1999] and subject to kinetic nucleation zones where sandstone chemical diagenesis occurs [*Hayes*, 1979].

5.2. Rock Hardness, Fracture Density, and Limits on Soil Production

In soil pits and on road cuts we observed fracture densities ranging on the order of <1 m in the typical Tyee formation. By contrast, average fracture spacing is more than an order of magnitude higher in the resistant Tyee (Figures S1 and S2.) We propose that the presence or absence of diagenetic strengthening materials within the Tyee Formation controls fracture density given that nearby highly fractured typical Tyee beds likely experienced a similar stress history. The sparsely fractured, resistant rocks beds are commonly devoid of soil and lack the topographic signature of trees found in the soil-mantled landscape underlain by the typical Tyee (Figure 9). *Heimsath et al.* [2001] posited that the distribution of unweathered bedrock in the OCR limited soil production and transport processes by preventing tree roots and burrowers from penetrating resistant rock. This connection between rock properties and biotic weathering mechanisms implies that fracture density may control soil production mechanisms in resistant beds of the Tyee Formation.

Tree roots penetrate cracks in cliff faces and grow in rock with very little to no soil, although the roots are generally associated with rock fissures [*Matthes-Sears and Larson*, 1995]. Bedrock-to-soil production mechanisms via tree roots range from the cantilever beam-like leverage exerted by large diameter trees during windstorms [*Lutz*, 1960] to simple displacement via lift forces generated by roots extending along horizontal bedding planes. *Lutz* [1960] measured tree-induced movement of rocks weighing up to 4.5×10^3 kg when compiling data on the maximum movement of rocks by tree roots. Assuming a bedrock density of 2.3 g cm^{-3} [*Reneau and Dietrich*, 1991] for the Tyee Formation, a vertical fracture density of 3 m, and a horizontal bed spacing of 1 m, the calculated mass for a 9 m^3 block of rock is 21×10^3 kg, which is more

than 4 times *Lutz*'s [1960] maximum measured value of 4.5×10^3 kg. Specifically, a tree root extending along a horizontal bedding plane below the rock block exerts a force equal to

$$F = m_r \times a_g \quad (7)$$

where m_r is the rock mass and a_g is the acceleration due to gravity. To lift a 9 m^3 block of the resistant Tyee, a root would need to exert a force of $\sim 2.0 \times 10^5$ N. Tree roots along a horizontal plane have been observed to exert a radial pressure on the surrounding rock, and these radial pressures have been measured up to 0.91 MPa [*Bennie*, 1996]. Thus, in order to lift a 9 m^3 block of Tyee sandstone, root area would need to exceed 2 m^2 (equivalent to a diameter of over 0.5 m), which exceeds the maximum diameter of the largest roots found in the OCR. In comparison, we executed the same analysis for the typical Tyee, with an average fracture spacing of 0.59 m (Figure S2). By only varying the fracture spacing in the calculations, we arrive at a calculated volume of 0.35×10^3 m^3 and a mass of 0.8×10^3 kg (dimensions of 0.59 $m^2 \times 1$ m). Thus, to lift an average typical Tyee block, a root would need to exert a force of 0.08 MPa, an order of magnitude lower than maximum measured tree root radial pressures that have been previously measured [*Bennie*, 1996]. We calculated that a minimum root diameter of 0.1 m is required to lift an average size block of the typical Tyee; we commonly observe roots of this size in exposed Douglas fir root masses. These simple calculations suggest that rock strength controls on fracture density also affect bedrock detachment by tree roots, thus representing a limit on tree roots as a soil production and erosion agent.

5.3. Resistant Rock Beds, Topographic Metrics, and Landscape Evolution

Given the prevalence of cosmogenic radionuclides for measuring erosion rates, numerous studies assess the extent to which erosion varies with various topographic metrics, perhaps most commonly average gradient. Interestingly, whole-watershed hillslope gradient and slope-area data do not show a significant difference between Franklin and Harvey watersheds despite the difference in relief between the two watersheds at the larger ridge and valley scale. Rather, the influence of resistant rock beds on local base level and the mechanics and rates of soil production becomes readily apparent when comparing slopes and slope drainage area plots at the subcatchment scale (Figures 4 and 6). Curiously, in the case of Franklin watershed, it appears that the combination of high-gradient nonsoil mantled slopes and lower gradient soil-mantled slopes perched above the resistant rock beds roughly balance the mean hillslope gradient in the adjoining soil-mantled Harvey watershed.

Conversely, longitudinal and chi profiles that traverse the length of the two watersheds show significant differences (Figures 5). Similarly, while valley width systematically increases as a power law function with drainage area in both watersheds, valleys are nearly 1.5 times wider in Harvey than in Franklin (Figure 7). Our results imply that whole-watershed gradient comparisons may be a potentially perilous analytical tool for making process-scale predictions.

In Franklin, the similarity in the slope drainage area plots between the two watersheds may simply result from the offsetting effect of slope differences in Franklin. Of note is the pronounced scaling break between drainage areas <1 km^2 and larger drainage areas (Figures 5 and 6), which suggests that a fundamental process signature, the debris-fluvial transition, is not suppressed by the resistant beds. *Duvall et al.* [2004] noted correlation in concavity indexes with variability in bedrock competence, with high concavities associated with the more resistant rocks. Not surprisingly, we see no similar relationship in Franklin, as unlike the *Duvall et al.* [2004] study, our watersheds do not cross a resistant rock lithology before transitioning to a weaker rock type further downstream but rather intermittently encounter resistant rock beds.

Topographic metrics describing hillslope gradients and slope drainage area relationships in Franklin provide insight into the evolution of channel profiles as resistant rock beds are exposed. Comparing slope-area plots within Franklin watershed, we observe a dramatic difference between subcatchments (Figures 6d and 6f). In F1, the exhumation of resistant rock beds has been ongoing for some time, such that only the upper half of the catchment remains perched above the beds. This contrasts with F3, in the northern part of the watershed, where the resistant rock beds are just beginning to emerge. We interpret the concave-up channel profile in catchment F1 as indicative of long-standing hard rock exposure in the southern part of Franklin watershed, while the catchment F3 (and nearby) hillslopes are responding to the newly exhumed beds, such that the resistant rock channel has yet to erode into a concave-up form.

Both the hillslope gradient and the hilltop curvature models predict that Franklin catchments perched above the resistant beds erode at approximately half the rate of Harvey catchments. The difference in erosion rate predictions for the gradient (equations (2) and (3)) and hilltop (equation (4)) models likely reflects model assumptions (e.g., 1-D versus 2-D solutions) and lidar processing choices, such as smoothing length scales. Thus, we assert that the models agree as to the magnitude of the erosion rate contrast.

By incorporating the hilltop curvature-erosion model results (equation (4)) within the dimensionless E^* and R^* framework (equations (2) and (3)), we can explore deviations from steady state. Given base level changes, hilltop curvature responds by sharpening in response to an increase in uplift and relaxing in response to a decrease in uplift rates [*Hurst et al.*, 2013a]. Our model results (Figure 8) suggest that Franklin watershed may be more transient than Harvey. As changes in absolute uplift rates propagate from channel to hillslope, slope gradients respond faster than drainage density and thus hillslope length [*Howard*, 1997]. Given the somewhat patchy presence of the resistant beds in Franklin, transience and basin reorganization seems likely. Visually, the topography of Franklin appears disorganized with respect to catchment orientations, basin shape, and drainage density (Figure 1), particularly when compared with the regularity of Harvey. Our results suggest that as the resistant beds emerged in the Franklin watershed, hillslope erosion slowed, hilltop curvatures relaxed, and hillslopes lengthened, with an expected trajectory that reverses the hysteresis imposed by a passing wave of increased uplift [*Hurst et al.*, 2013a].

We posit that elevated relief values in Franklin watershed result from the combination of resistant beds within individual small catchments, a large knickzone in mainstem Franklin, and the watershed-scale influence of changes in sediment supply and caliber propagating through the basin. In bedrock channels the rate of incision is proposed to depend on the grain size supplied to channels [*Sklar and Dietrich*, 1998, 2004]. In the individual catchments, the resistant beds set local base level and thus influence erosion rates and relief. Hillslope grain size distributions in paired catchments with contrasting erosion rates consistently exhibit a positive correlation between decreased erosion rates, grain size, and durability in multiple lithologic and climatic settings [*Marshall et al.*, 2009]. We speculate that in Franklin watershed, the resistant rock influences grains size distribution supply to the channel and, thus, incision rates in two ways: via modulation of the typical Tyee grain size distribution and by dint of the resistant Tyee weathering patterns. First, we expect sediment in slow eroding soil-mantled catchments perched above resistant beds to have a smaller overall grain size distribution and smaller median grain size and abrade faster than the sandstone with the same rock properties in a faster eroding watershed due to the longer weathering time in the soil [*Marshall et al.*, 2009; *Sweeney et al.*, 2012]. Second, we have observed two modes of resistant rock erosion: massive block failure or exfoliation of easily broken centimeter-scale rock flakes. The massive resistant rock blocks create immobile boulder fields in Franklin Creek and its tributaries, as they are too large for fluvial transport. In fact, we observe potholes on these massive blocks in Franklin Creek, suggestive of their long-lived nature. Overall, the combination of reduced grain size supply and caliber from perched watersheds and oversized supply from the resistant rock should result in a smaller range of incision effective grain sizes (tools) in Franklin watershed compared to the "typical" tool supply in Harvey.

In the Oregon Coast Range, the context of the Eocene submarine ramp depositional setting constrains modern-day geomorphic processes. Sand-silt ratios and structure control deep-seated landslides in the region, with large $>$1 km scale landslides correlating with increased silt to sand ratios and bedrock downdip locations [*Roering et al.*, 2005]. In contrast to the silt-dominated region, where the hills are effectively weaker and slide-prone, our sites within the sand-dominated proximal slope setting reveal diagenetic variations that can prop the landscape up and increase relief. Furthermore, our results imply several means by which we may incorporate rock properties into geomorphic process models. In landscapes where trees dominate sediment production, fracture density may limit soil production and control the extent of rock fall-dominated bedrock-to-mobile regolith production. Thus, we might expect that the peak soil production value (often defined as the soil production rate when soil depth is absent) in soil production models increases with fracture density. Furthermore, bedrock strength can directly enter tools-based models of fluvial and debris flow incision [e.g., *Sklar and Dietrich*, 2004; *Stock and Dietrich*, 2006].

Our results highlight the need to consider and even embrace petrologic (and in this case diagenetic) sources of bedrock variability. With the increasing availability of airborne lidar and open source tools for extracting topographic metrics such as channel steepness indexes, it is possible to attribute morphologic variability to

climate or tectonics when instead grain-scale differences may control soil production (sections 4.3 and 5.2) or hillslope and channel erosion processes (sections 4.2–4.4 and 5.3). As such, lithologic variability is a key consideration when interpreting landscape form and calibrating process models.

6. Conclusions

We have exploited the contrasts between resistant and nonresistant rock exposures in two adjoining watersheds in the well-studied Oregon Coast Range to examine how rock properties influence the mechanical properties of rock and thus geomorphic function and landscape processes. In contrast to most studies that referenced *Gilbert*'s [1877] early observations demonstrating that hard rock creates steeper landscapes, lidar data allows us to quantify the scale over which hard rock modulates to local- and watershed-scale geomorphic form and function. In single lithologies, we commonly make an assumption of uniformity and ignore intralithologic variation. In this study, we show that rock property variation over small spatial extents within a single lithology may have profound implications for landscape evolution.

We have demonstrated that trace differences in diagenetic processes, specifically a combination of fibrous clays and chlorite cements, manifest as 1 to 10 m thick bands of resistant bedrock that are continuous yet noncontiguous in our study area. We utilized 1-D spectral analysis to document the lack of a biotic signature imparted by trees roots in the nonsoil mantled resistant rock, which contrasts with the biotic signature pervasive in the typical bedrock. Based on simple mass calculations, we established that rock control on fracture density may limit bedrock-to-soil production via detachment. We used theoretical erosion-topography models to predict erosion rates for catchments perched above the resistant beds and found that these values are approximately half those observed for nearby hillslopes unaffected by resistant beds. We demonstrated that thin bands of resistant rock control relief at the watershed scale for >1 My periods.

Our findings suggest that even meter-scale expressions of lithologic variability may control geomorphic function enough to challenge the appropriateness of parameterizing process models under the assumption of uniform behavior within a single lithology.

Acknowledgments

The authors thank Adam Booth, Scott Eaton, and Christine May for the many stimulating and insightful discussions. Insightful comments from TC Hales, two anonymous reviewers, and Associate Editor Simon Mudd greatly improved the manuscript. DOGAMAI lidar data are freely available for download at http://www.opentopography.org/. J.A.M. and J.R.R. were supported by NSF EAR-0952186.

References

Aalto, R., T. Dunne, and J. L. Guyot (2006), Geomorphic controls on Andean denudation rates, *J. Geol.*, *114*(1), 85–99, doi:10.1086/498101.

Ahnert, F. (1987), Approaches to dynamic equilibrium in theoretical simulations of slope development, *Earth Surf. Processes Landforms*, *12*(1), 3–15, doi:10.1002/esp.3290120103.

Aldrich, F. T. (1972), A chorological analysis of the grass balds in the Oregon Coast Range, PhD dissertation, Oregon State Univ., 31 May.

Allen, G. H., J. B. Barnes, T. M. Pavelsky, and E. Kirby (2013), Lithologic and tectonic controls on bedrock channel form at the northwest Himalayan front, *J. Geophys. Res. Earth Surf.*, *118*, 1806–1825, doi:10.1002/jgrf.20113.

Al-Tahini, A., C. Sondergeld, and C. Rai (2006), The effect of cementation on the mechanical properties of sandstones, *SPE Reservoir Eval. Eng.*, *94*(6), 306–316.

Baldwin, E. (1961), Geologic map of the lower Umpqua River area, Oregon, *US Geol. Survey Map OM, 204*, no. 1963, scale 1:62:500, Washington D. C.

Bennie, A. T. P. (1996), Growth and mechanical impedance, in *Plant Roots: The Hidden Half*, edited by Y. Waisel, A. Eshel, and U. Kafkafi, pp. 393–414, Marcel Dekker, Inc., New York.

Bierman, P., E. Clapp, K. Nichols, A. Gillespie, and M. Caffee (2001), Using cosmogenic nuclide measurements in sediments to understand background rates of erosion and sediment transport, in *Landscape Erosion and Evolution Modeling*, edited by R. S. Harmon and W. M. Doe, pp. 89–116, Kluwer, New York.

Butenuth, C. (1997), Comparison of tensile strength values of rocks determined by point load and direct tension tests, *Rock Mech. Rock Eng.*, *30*(1), 65–72, doi:10.1007/BF01020114.

Callen, R. (1984), Clays of the palygorskite-sepiolite group: Depositional environment, age and distribution, *Dev. Sedimentol.*, *37*, 1–37, doi:10.1016/S0070-4571(08)70027-X.

Chan, M. A. (1985), Correlations of diagenesis with sedimentary facies in Eocene sandstones, western Oregon, *J. Sediment. Res.*, *55*(3), 0322–0333, doi:10.1306/212F86B6-2B24-11D7-8648000102C1865D.

Chan, M. A., and R. H. Dott Jr. (1983), Shelf and deep-sea sedimentation in Eocene forearc basin, western Oregon-fan or non-fan, *Am. Assoc. Pet. Geol. Bull.*, *67*(11), 2100–2116.

Clarke, B. A., and D. W. Burbank (2010), Bedrock fracturing, threshold hillslopes, and limits to the magnitude of bedrock landslides, *Earth Planet. Sci. Lett.*, *297*(3-4), 577–586, doi:10.1016/j.epsl.2010.07.011.

DiBiase, R. A., K. X. Whipple, A. M. Heimsath, and W. B. Ouimet (2010), Landscape form and millennial erosion rates in the San Gabriel Mountains, CA, *Earth Planet. Sci. Lett.*, *289*, 134–144, doi:10.1016/j.epsl.2009.10.036.

DiBiase, R. A., A. M. Heimsath, and K. X. Whipple (2012), Hillslope response to tectonic forcing in threshold landscapes, *Earth Surf. Processes Landforms*, *37*(8), 855–865, doi:10.1002/esp.3205.

Dietrich, W. E., and T. Dunne (1978), Sediment budget for a small catchment in mountainous terrain, *Z. Geomorphol. N.F.*, *29*, 191–206, doi:10.1007/s10069-002-0008-0.

Dietrich, W. E., D. G. Bellugi, L. S. Sklar, J. D. Stock, A. M. Heimsath, and J. J. Roering (2003), Geomorphic transport laws for predicting landscape form and dynamics, in *Prediction in Geomorphology*, *Geophys. Monogr. Ser.*, vol. 135, edited by P. R. Wilcock and R. M. Iverson, pp. 103–132, AGU, Washington, D. C.

Dott, R. H., Jr. (1966), Eocene deltaic sedimentation at Coos Bay, Oregon: Jour, *J. Geol.*, *74*, 373–420.

Dumitru, T. A., W. G. Ernst, J. E. Wright, J. L. Wooden, R. E. Wells, L. P. Farmer, A. J. R. Kent, and S. A. Graham (2012), Eocene extension in Idaho generated massive sediment floods into the Franciscan trench and into the Tyee, Great Valley, and Green River basins, *Geology*, *41*(2), 187–190, doi:10.1130/G33746.1.

Duvall, A., E. Kriby, and D. Burbank (2004), Tectonic and lithologic controls on bedrock channel profiles and processes in coastal California, *J. Geophys. Res.*, *109*, F03002, doi:10.1029/2003JF000086.

Ferrier, K. L., J. T. Perron, S. Mukhopadhyay, M. Rosener, J. D. Stock, K. L. Huppert, and M. Slosberg (2013), Covariation of climate and long-term erosion rates across a steep rainfall gradient on the Hawaiian island of Kauaʻi, *Geol. Soc. Am. Bull.*, *125*(7-8), 1146–1163, doi:10.1130/B30726.1.

Franklin, J. F., and C. T. T. Dyrness (1988), *Natural Vegetation of Oregon and Washington*, US Government Printing Office, Washington, D. C.

Gabet, E. J., and S. M. Mudd (2010), Bedrock erosion by root fracture and tree throw: A coupled biogeomorphic model to explore the humped soil production function and the persistence of hillslope soils, *J. Geophys. Res.*, *115*, F04005, doi:10.1029/2009JF001526.

Galan, E. (1996), Properties and applications of palygorskite-sepiolite clays, *Clay Miner.*, *31*(4), 443–453, doi:10.1180/claymin.1996.031.4.01.

Galloway, W. E. (1974), Deposition and diagenetic alteration of sandstone in northeast Pacific arc-related basins: Implications for graywacke genesis, *Geol. Soc. Am. Bull.*, *85*(3), 379, doi:10.1130/0016-7606(1974)85<379:DADAOS>2.0.CO;2.

Galloway, W. E. (1979), Diagenetic control of reservoir quality in arc-derived sandstones: Implications for petroleum exploration, *Soc. Econ. Paleontol. Mineral. Spec. Publ.*, *26*, 251–261.

Gilbert, G. K. (1877), *Report on the Geology of the Henry Mountains: US Geographical and Geological Survey of the Rocky Mountain Region*, Gov. Print Off., Washington, D. C.

Hack, J. (1957), Studies of longitudinal stream profiles in Virginia and Maryland, *U.S. Geol. Surv. Prof. Pap.*, 294-B, 94 pp.

Hack, J. (1973), Drainage adjustment in the Appalachians, in *Fluvial Geomorphology*, edited by M. Morisawa, pp. 51–69, State Univ. of New York, Binghamton.

Hanley, J. T. (1977), Fourier analysis of the Catawba Mountain knolls, Roanoke county, Virginia, *J. Int. Assoc. Math. Geol.*, *9*(2), 159–163, doi:10.1007/BF02312510.

Harrison, J. M., and C.-P. P. Lo (1996), PC-based two-dimensional discrete Fourier transform programs for terrain analysis, *Comput. Geosci.*, *22*(4), 419–424.

Hawthorne, N. (1854), Sketches from memory: The notch of the White Mountains, in *Mosses from an Old Manse*, p. 256, Mifflin and Company, The Riverside Press Cambridge, Boston, New York. [Retrieved from: http://www.eldritchpress.org/nh/sfm.html].

Hayes, J. (1979), Sandstone diagenesis—The hole truth, *SEPM Spec. Publ.*, *26*, 127–139.

Heimsath, A. M., W. E. Dietrich, K. Nishiizumi, and R. C. Finkel (1997), The soil production function and landscape equilibrium, *Nature*, *388*, 21–24, doi:10.1144/SP312.8.

Heimsath, A. M., W. E. Dietrich, K. Nishiizumi, and R. C. Finkel (2001), Stochastic processes of soil production and transport: Erosion rates, topographic variation and cosmogenic nuclides in the Oregon Coast Range, *Earth Surf. Processes Landforms*, *26*(5), 531–552, doi:10.1002/esp.209.

Heimsath, A. M., R. A. DiBiase, and K. X. Whipple (2012), Soil production limits and the transition to bedrock-dominated landscapes, *Nat. Geosci.*, *5*(3), 210–214, doi:10.1038/ngeo1380.

Heller, P. L., and W. R. Dickinson (1985), Submarine ramp facies model for delta-fed, sand-rich turbidite systems, *Am. Assoc. Pet. Geol. Bull.*, *69*(6), 960.

Heller, P. L., and P. T. Ryberg (1983), Sedimentary record of subduction to forearc transition in the rotated Eocene basin of western Oregon, *Geology*, *11*(7), 380, doi:10.1130/0091-7613(1983)11<380:SROSTF>2.0.CO;2.

Heller, P. L., Z. E. Peterman, J. R. O'Neil, and M. Shafiqullah (1985), Isotopic provenance of sandstones from the Eocene Tyee Formation, Oregon Coast Range, *Geol. Soc. Am. Bull.*, *96*, 770–780, doi:10.1130/0016-7606(1985)96<770:IPOSFT>2.0.CO;2.

Heller, P. L., R. W. Tabor, and C. A. Suczek (1987), Paleogeographic evolution of the United States Pacific Northwest during Paleogene time, *Can. J. Earth Sci.*, *24*(8), 1652–1667, doi:10.1139/e87-159.

Heller, P. L., P. R. Renne, and J. R. O'Neil (1992), River mixing rate, residence time, and subsidence rates from isotopic indicators: Eocene sandstones of the US Pacific Northwest, *Geology*, *20*(12), 1095–1098, doi:10.1130/0091-7613(1992)020<1095.

Howard, A. D. (1997), Badland morphology and evolution: Interpretation using a simulation model, *Earth Surf. Processes Landforms*, *22*(3), 211–227, doi:10.1002/(SICI)1096-9837(199703)22:3<211::AID-ESP749>3.0.CO;2-E.

Howard, A. D. (1998), Long profile development of bedrock channels: Interaction of weathering, mass wasting, bed erosion, and sediment transport, in *Rivers Over Rock: Fluvial Processes in Bedrock Channels*, edited by K. J. Tinkler and E. E. Wohl, *Geophys. Monogr. Ser.*, vol. 107, pp. 297–319, AGU, Washington, D. C.

Hurst, M. D., S. M. Mudd, R. Walcott, M. Attal, and K. Yoo (2012), Using hilltop curvature to derive the spatial distribution of erosion rates, *J. Geophys. Res.*, *117*, F02017, doi:10.1029/2011JF002057.

Hurst, M. D., S. M. Mudd, M. Attal, and G. Hilley (2013a), Hillslopes record the growth and decay of landscapes, *Science*, *341*(6148), 868–871, doi:10.1126/science.1241791.

Hurst, M. D., S. M. Mudd, K. Yoo, M. Attal, and R. Walcott (2013b), Influence of lithology on hillslope morphology and response to tectonic forcing in the northern Sierra Nevada of California, *J. Geophys. Res. Earth Surf.*, *118*, 832–851, doi:10.1002/jgrf.20049.

Hutcheon, I. (1983), Diagenesis 3. Aspects of the diagenesis of coarse-grained siliciclastic rocks, *Geosci. Can.*, *10*(1), 4–14.

Kasahara, T., and S. M. Wondzell (2003), Geomorphic controls on hyporheic exchange flow in mountain streams, *Water Resour. Res.*, *39*(1), 1005, doi:10.1029/2002WR001386.

Kelsey, H. M., D. C. Engebretson, C. E. Mitchell, and R. L. Ticknor (1994), Topographic form of the Coast Ranges of the Cascadia margin in relation to coastal uplift rates and plate subduction, *J. Geophys. Res.*, *99*, 12,245–12,255, doi:10.1029/93JB03236.

Kirby, E., and K. X. Whipple (2001), Quantifying differential rock-uplift rates via stream profile analysis, *Geology*, *29*(5), 415–418.

Kirby, E., and K. X. Whipple (2012), Expression of active tectonics in erosional landscapes, *J. Struct. Geol.*, *44*, 54–75, doi:10.1016/j.jsg.2012.07.009.

Kobor, J., and J. Roering (2004), Systematic variation of bedrock channel gradients in the central Oregon Coast Range: Implications for rock uplift and shallow landsliding, *Geomorphology*, *62*(3), 239–256.

Korup, O., and F. Schlunegger (2009), Rock-type control on erosion-induced uplift, eastern Swiss Alps, *Earth Planet. Sci. Lett.*, *278*(3-4), 278–285, doi:10.1016/j.epsl.2008.12.012.

Lague, D., and P. Davy (2003), Constraints on the long-term colluvial erosion law by analyzing slope-area relationships at various tectonic uplift rates in the Siwaliks Hills (Nepal), *J. Geophys. Res.*, *108*(B2), 2129, doi:10.1029/2002JB001893.

Lovell, J. (1969), Tyee formation; a study of proximality in turbidites, *J. Sediment. Res.*, *39*(3), 935–953.
Lovell, J., and J. Rogers (1969), Tyee Formation: Undeformed turbidites and their lateral equivalents: Mineralogy and paleogeography, *Geol. Soc. Am. Bull.*, *80*(1), 9–22.
Lutz, H. (1960), Movement of rocks by uprooting of forest trees, *Am. J. Sci.*, *258*(10), 752–756.
Marshall, J. A., M. Attal, L. S. Sklar, C. S. Riebe, M. D. Hurst, S. M. Mudd, and K. Yoo (2009), The effect of erosion rate on hillslope rock fragment production: Implications for supply of bedload material to channels, *Eos Trans. AGU*, *90*(52), Fall Meet. Suppl., Abstract EP51B-0594.
Matthes-Sears, U., and D. Larson (1995), Rooting characteristics of trees in rock: A study of Thuja occidentalis on cliff faces, *Int. J. Plant Sci.*, *156*(5), 679–686.
May, C., J. Roering, L. Eaton, and K. Burnett (2013), Controls on valley width in mountainous landscapes: The role of landsliding and implications for salmonid habitat, *Geology*, *41*, 503–506, doi:10.1130/g33979.1.
Montgomery, D. R. (2001), Slope distributions, threshold hillslopes, and steady-state topography, *Am. J. Sci.*, *301*(4-5), 432–454, doi:10.2475/ajs.301.4-5.432.
Montgomery, D. R., and M. T. Brandon (2002), Topographic controls on erosion rates in tectonically active mountain ranges, *Earth Planet. Sci. Lett.*, *201*(3-4), 481–489, doi:10.1016/S0012-821X(02)00725-2.
Montgomery, D. R., and E. Foufoula-Georgiou (1993), Channel network source representation using digital elevation models, *Water Resour. Res.*, *29*, 3925–3934, doi:10.1029/93WR02463.
Moore, J. R., J. W. Sanders, W. E. Dietrich, and S. D. Glaser (2009), Influence of rock mass strength on the erosion rate of alpine cliffs, *Earth Surf. Processes Landforms*, *34*(10), 1339–1352, doi:10.1002/esp.1821.
Mudd, S. M., M. Attal, D. T. Milodowski, S. W. D. Grieve, and D. A. Valters (2014), A statistical framework to quantify spatial variation in channel gradients using the integral method of channel profile analysis, *J. Geophys. Res. Earth Surf.*, *119*, 138–152, doi:10.1002/2013JF002981.
Naiman, R., and R. Bilby (Eds.) (1998), *River Ecology and Management: Lessons From the Pacific Coastal Ecoregion*, Springer Verlag, New York.
Orr, E. L., W. N. Orr, and E. M. Baldwin (1992), *Geology of Oregon*, 254 pp., Kendall/ Hunt, Dubuque, Iowa.
Ouimet, W. B., K. X. Whipple, and D. E. Granger (2009), Beyond threshold hillslopes: Channel adjustment to base-level fall in tectonically active mountain ranges, *Geology*, *37*(7), 579–582, doi:10.1130/G30013A.1.
Perron, J. T., and L. Royden (2013), An integral approach to bedrock river profile analysis, *Earth Surf. Processes Landforms*, *38*, 570–576, doi:10.1002/esp.3302.
Perron, J. T., J. W. Kirchner, and W. E. Dietrich (2008), Spectral signatures of characteristic spatial scales and nonfractal structure in landscapes, *J. Geophys. Res.*, *113*, F04003, doi:10.1029/2007JF000866.
Perron, J. T., J. W. Kirchner, and W. E. Dietrich (2009), Formation of evenly spaced ridges and valleys, *Nature*, *460*(7254), 502–505, doi:10.1038/nature08174.
Priestley, M. B. (1981), *Spectral Analysis and Time Series*, *Univariate series*, vol. 1, Academic Press, New York.
Rayner, J. (1972), The application of harmonic and spectral analysis to the study of terrain, in *Spatial Analysis in Geomorphology*, edited by R. J. Chorley, pp. 283–302, Methuen, London.
Reneau, S. L., and W. E. Dietrich (1991), Erosion rates in the southern oregon coast range: Evidence for an equilibrium between hillslope erosion and sediment yield, *Earth Surf. Processes Landforms*, *16*, 307–322, doi:10.1002/esp.3290160405.
Richards, M., M. Bowman, and H. Reading (1998), Submarine-fan systems I: Characterization and stratigraphic prediction, *Mar. Pet. Geol.*, *15*, 689–717, doi:10.1016/S0264-8172(98)00036-1.
Roering, J. J. (2008), How well can hillslope evolution models "explain" topography? Simulating soil transport and production with high-resolution topographic data, *Geol. Soc. Am. Bull.*, *120*, 1248–1262, doi:10.1130/B26283.1.
Roering, J. J., J. W. Kirchner, and W. E. Dietrich (1999), Evidence for nonlinear, diffusive sediment transport on hillslopes and implications for landscape morphology, *Water Resour. Res.*, *35*, 853–870, doi:10.1029/1998WR900090.
Roering, J. J., J. W. Kirchner, and W. E. Dietrich (2005), Characterizing structural and lithologic controls on deep-seated landsliding: Implications for topographic relief and landscape evolution in the Oregon Coast Range, USA, *Geol. Soc. Am. Bull.*, *117*, 654–668, doi:10.1130/B25567.1.
Roering, J. J., J. T. Perron, and J. W. Kirchner (2007), Functional relationships between denudation and hillslope form and relief, *Earth Planet. Sci. Lett.*, *264*, 245–258, doi:10.1016/j.epsl.2007.09.035.
Roering, J. J., J. Marshall, A. M. Booth, M. Mort, and Q. Jin (2010), Evidence for biotic controls on topography and soil production, *Earth Planet. Sci. Lett.*, *298*(1–2), 183–190, doi:10.1016/j.epsl.2010.07.040.
Rogers, J. (1969), Tyee formation: Undeformed turbidites and their lateral equivalents: Mineralogy and paleogeography: Discussion, *Geol. Soc. Am. Bull.*, *80*(10), 2129, doi:10.1130/0016-7606(1969)80[2129:TFUTAT]2.0.CO;2.
Rogers, J., and K. Richardson (1964), Thorium and uranium contents of some sandstones, *Geochim. Cosmochim. Acta*, *28*(12), 2005–2011.
Ryu, I., and A. R. Niem (1999), Sandstone diagenesis, reservoir potential, and sequence stratigraphy of the Eocene Tyee Basin, Oregon, *J. Sediment. Res.*, *69*(1), 384–393, doi:10.1306/D42689F5-2B26-11D7-8648000102C1865D.
Schmidt, K. M., and D. R. Montgomery (1995), Limits to relief, *Science*, *270*(5236), 617–620, doi:10.1126/science.270.5236.617.
Seidl, M., and W. Dietrich (1992), The problem of channel erosion into bedrock, *Catena*, *23*(Supplement), 101–104.
Selby, M. (1993), *Hillslope Materials and Processes*, 2nd ed., Oxford Univ. Press, Oxford.
Simpson, R. W. R., and A. Cox (1977), Paleomagnetic evidence for tectonic rotation of the Oregon Coast Range, *Geology*, doi:10.1130/0091-7613(1977)5<585:PEFTRO>2.0.CO;2.
Sklar, L. S., and W. E. Dietrich (1998), River longitudinal profiles and bedrock incision models: Stream power and the influence of sediment supply, in *Rivers Over Rock: Fluvial Processes in Bedrock Channels*, vol. 107, edited by K. J. Tinkler and E. E. Wohl, pp. 237–260, *Geophys. Monogr. Ser.*, AGU, Washington, D. C.
Sklar, L. S., and W. E. Dietrich (2001), Sediment and rock strength controls on river incision into bedrock, *Geology*, *29*(12), 1087–1090, doi:10.1130/0091-7613(2001)029<1087:SARSCO>2.0.CO;2.
Sklar, L. S., and W. E. Dietrich (2004), A mechanistic model for river incision into bedrock by saltating bed load, *Water Resour. Res.*, *40*, W06301, doi:10.1029/2003WR002496.
Sklar, L. S., and W. E. Dietrich (2006), The role of sediment in controlling steady-state bedrock channel slope: Implications of the saltation–abrasion incision model, *Geomorphology*, *82*, 58–83, doi:10.1016/j.geomorph.2005.08.019.
Snavely, P. D., H. C. Wagner, and N. S. MacLeod (1964), Rhythmic-bedded eugeosynclinal deposits of the Tyee formation, Oregon Coast Range, *Kans. Geol. Surv. Bull.*, *169*, 461–480.
Snyder, N. P., K. X. Whipple, G. E. Tucker, and D. J. Merritts (2000), Landscape response to tectonic forcing: Digital elevation model analysis of stream profiles in the Mendocino triple junction region, northern California, *Geol. Soc. Am. Bull.*, *112*, 1250–1263, doi:10.1130/0016-7606(2000)112<1250:LRTTFD>2.0.CO;2.

Stock, J. D., and W. E. Dietrich (2003), Valley incision by debris flows: Evidence of a topographic signature, *Water Resour. Res.*, *39*(4), 1089, doi:10.1029/2001WR001057.

Stock, J. D., and W. E. Dietrich (2006), Erosion of steepland valleys by debris flows, *Geol. Soc. Am. Bull.*, *118*(9–10), 1125–1148, doi:10.1130/B25902.1.

Stock, J. D., D. R. Montgomery, B. D. Collins, W. E. Dietrich, and L. Sklar (2005), Field measurements of incision rates following bedrock exposure: Implications for process controls on the long profiles of valleys cut by rivers and debris flows, *Geol. Soc. Am. Bull.*, *117*(1–2), 174, doi:10.1130/B25560.1.

Sweeney, K. E., J. J. Roering, P. Almond, and T. Reckling (2012), How steady are steady-state landscapes? Using visible-near-infrared soil spectroscopy to quantify erosional variability, *Geology*, *40*(9), 807–810, doi:10.1130/G33167.1.

VanLaningham, S. (2006), The effects of rock uplift and rock resistance on river morphology in a subduction zone forearc, Oregon, USA, *Earth Surf. Processes Landforms*, *31*(10), 1257–1279, doi:10.1002/esp.

Vutukuri, V. S., R. D. Lama, and S. S. Saluja (1974), *Handbook on Mechanical Properties of Rocks, Testing Techniques and Results*, *Series on Rock and Soil Mechanics*, vol. 1, pp. 105–115, Trans. Tech Publishers, Bay Village, Ohio.

Weaver, C. E. (2000), Origin and geologic implications of the palygorskite of the SE United States, in *Palygorskite-Sepiolite: Occurrences, Genesis and Uses*, edited by A. Singer and E. Galan, Elsevier B.V., Amsterdam.

Wells, R. E., and P. L. Heller (1988), The relative contribution of accretion, shear, and extension to Cenozoic tectonic rotation in the Pacific Northwest, *Geol. Soc. Am. Bull.*, *100*, 325–338, doi:10.1130/0016-7606(1988)100<0325:TRCOAS>2.3.CO;2.

Wheatcroft, R. A., and C. K. Sommerfield (2005), River sediment flux and shelf sediment accumulation rates on the Pacific Northwest margin, *Cont. Shelf Res.*, *25*(3), 311–332, doi:10.1016/j.csr.2004.10.001.

Whipple, K. X. (2004), Bedrock rivers and the geomorphology of active orogens, *Annu. Rev. Earth Planet. Sci.*, *32*, 151–185, doi:10.1146/annurev.earth.32.101802.120356.

Whipple, K. X., E. Kirby, and S. H. Brocklehurst (1999), Geomorphic limits to climate-induced increases in topographic relief, *Nature*, *401*, 39–43, doi:10.1038/43375.

Whipple, K. X., C. Wobus, B. Crosby, E. Kirby, and D. Sheehan (2007), New tools for quantitative geomorphology: Extraction and interpretation of stream profiles from digital topographic data, GSA Short Course, 506.

Willett, S., S. McCoy, J. Perron, L. Goren, and C. Chen (2014), Dynamic reorganization of river basins, *Science*, *343*(6175), doi:10.1126/science.1248765.

Wobus, C., K. X. Whipple, E. Kirby, N. Snyder, J. Johnson, K. Spyropolou, B. Crosby, and D. Sheehan (2006), Tectonics from topography: Procedures, promise, and pitfalls, in *Tectonics, Climate, and Landscape Evolution*, edited by S. D. Willett et al., *Geol. Soc. Am. Spec. Pap.*, *398*, 55–74, doi:10.1130/2006.2398(04).

Wood, J. (1996), The geomorphological characterisation of digital elevation models, PhD dissertation, Univ. of Leicester, U. K.

Yatsu, E. (1971), Landform material science, rock control in geomorphology, in *Proceedings, 1st Guelph Symposium on Geomorphology*, vol. 1, pp. 49–73, Univ. of Guelph Geographical Publication, Ontario.

Yatsu, E. (1988), *The Nature of Weathering: An Introduction*, 624 pp., Sozosha, Tokyo.